Positive Muon Studies of Magnetic Materials

Contents

Positive Muon Studies of Magnetic Materials

ABSTRACT

Bruce DoBos Patterson

Polarized positive muons (μ^+) are stopped in magnetic materials, and the μ^+ precession is observed via the muon's asymmetric decay to a positron. The precession frequency is a measure of the local magnetic field at the μ^+. Relaxation of the μ^+ spin is caused by spatially or time-varying local fields.

The local field at a stopped μ^+ in ferromagnetic nickel is measured. From this measurement, the hyperfine field seen by an interstitial μ^+ due to its contact interaction with polarized screening electrons is inferred to be -0.66kG. A discussion of this value in terms of a simple model for the screening configuration is presented.

Critical spin fluctuations in Ni at temperatures just above the Curie point rapidly relax the μ^+ spin. The temperature and external magnetic field dependence of the relaxation rate is determined experimentally. A theory for the relaxation rate is presented which demonstrates the importance of the hyperfine and dipolar interactions of the μ^+ with its Ni host.

Preliminary results on μ^+ studies in ferromagnetic iron and cobalt are also discussed.

I. INTRODUCTION

A. The Positive Muon and the μSR Technique

The positive muon or μ^+ is an elementary particle with unit positive charge. It was first observed as a component of cosmic rays, and with the advent of large accelerators it could be produced artifically. A brief summary of its properties is presented in Table 1.

Because it has spin 1/2, the μ^+ has a magnetic dipole moment but no electric quadrupole moment. Its mass of 1/9 the proton mass is such that one may often think of the μ^+ simply as a light proton. The μ^+ is unstable, however, decaying into a positron and two neutrinos with a mean lifetime of 2.2 μsec. The gyromagnetic ratio and lifetime of the μ^+ are such that it precesses one revolution in its lifetime in a field of 34 gauss. Laboratory fields of this order of magnitude are easily produced and controlled.

The parent of the μ^+ is a positive pion. When the pion decays to a μ^+, the μ^+ is polarized with its spin anti-parallel to its momentum. One thus knows the initial orientation of the muon's moment. When the μ^+ decays, the positron is emitted preferentially along the muon's spin direction, so by noting the direction of positron emission one knows something about the final orientation of the muon spin. It is possible, therefore, to follow the evolution of the muon spin direction with time.

This ability to follow the muon spin and the convenient magnitude of its lifetime and gyromagnetic ratio make the μ^+ a

PROPERTIES OF THE μ^+

Spin: 1/2

Mass: $m_\mu = 207\ m_e = 0.113 m_p$

Magnetic Moment: $\mu_\mu = 1/207\ \mu_B = 3.18\ \mu_p$

Gyromagnetic Ratio: $\gamma_\mu = 13.6$ MHz/kGauss

Lifetime: $\tau_\mu = 2.20$ μsec

Decay Mode: $\mu^+ \rightarrow e^+ + \nu_e + \bar{\nu}_\mu$

Table 1. The numerical values stated are known to many more significant digits than shown. See Ref. 1.

valuable magnetic probe of matter. By observing the precession of the μ^+ stopped in a sample and determining the frequency of precession, one may, via the known gyromagnetic ratio[1], find the local magnetic field acting on the μ^+. This is the muon spin rotation or "μSR" technique.[2]

It is believed that the μ^+ enters most solid materials as an interstitial impurity. In solids which contain large amounts of hydrogen, the μ^+ tends to replace a proton.[3] In an insulator, the μ^+ captures an electron[4] to form muonium ($\mu^+ - e^-$), while in a metal it attracts neighboring conduction electrons, forming[5] an unbound screening cloud. These situations represent electronic impurity states not found in the pure host. The μSR technique thus allows access to one of the simplest conceivable impurity problems: a point charge in an otherwise pure host. It contrasts with techniques like x-ray and neutron diffraction, which are designed to study pure materials, not isolated impurities.

The μSR technique bears a strong resemblance to the nuclear magnetic resonance technique (NMR) in that they both measure the local magnetic field at a microscopic probe. NMR, however, requires the absorption of a macroscopic amount of power, necessitating a relatively high concentration of resonant nuclei. The μSR technique operates in the extreme dilute limit of one μ^+ in the sample at a time.

The fact that the μ^+ occupies an interstitial site also sets it apart from most other types of probe. Conventional probes are usually the electrons or nucleus of a host atom or substitutional impurity. This difference is especially significant for the case

of ferromagnets where a nuclear probe and an interstitial probe see drastically different local fields.

B. Protons and μ^+ in Metals

The electronic structure of a μ^+ impurity and a proton impurity are identical if one neglects the small difference in the reduced masses of associated electrons. Proton magnetic resonance (PMR) makes available information similar to that obtained from a μSR experiment.

PMR has been performed on a large number of solids containing protons. Most of these are insulating compounds containing large amounts of hydrogen. Although the μSR technique can be applied to such systems[3], it is most valuable in systems where PMR is not feasible, such as the metal-dilute impurity system.

Many metals can be charged with enough hydrogen to make PMR observable. Typical samples are transition and rare earth metal hydrides $M\text{-}H_x (x > .1)$. Such high hydrogen concentrations are required to have a sufficient number of resonant nuclei in the skin depth of the sample. Although these experiments are far from the dilute limit, it is instructive to see what type of information has been learned.

Properties under study with PMR in metal-hydrogen systems include: 1) the Knight or chemical shift[6] of the PMR frequency (which reveals details of the electronic structure of the impurity state) 2) the position of the protons in the host lattice (as determined by a careful measurement of the static PMR linewidth) and 3) the proton diffusion rate (as measured by the motional narrowing[7] of the PMR line).

The PMR frequency shifts for several hydrides have been measured[8-14] and most are compatible with the picture of an inter-

stitial proton surrounded by an unbound screening cloud. An exception is the case[15] of Ta-H, where hydrogen atoms make partial covalent bonds with the host atoms.

The proton sites in a few hcp and fcc metal lattices have been determined [10,12,16,17] via PMR. These results together with neutron diffraction studies [18,19] demonstrate that protons tend to occupy the octahedral and/or tetrahedral interstitial sites in these lattices. It is difficult to extrapolate this data to the dilute limit because of the existence of phase changes which accompany changes in the hydrogen concentration.

PMR studies [10,15,20-23] in several hydrides show line widths which become suddenly narrow above a fairly well defined threshold temperature. Above this temperature, the protons are rapidly diffusing, averaging out the effect of static microscopic inhomogenieties. This threshold temperature is usually of the order of a few hundred K.

The μSR technique has been applied to a few metals so far with interesting results. Because only one muon is in the sample at a time, it is definitely an isolated impurity which is under study. Knight shifts of μ^+ in various metals have been measured[24]; a theoretical interpretation of this data is presented subsequently.

Several studies of μ^+ diffusion in metals have been performed. The muon's activation energy and diffusion constant in copper have been determined[25] by observing the temperature dependent motional narrowing of the static dipolar linewidth. In a similar study[26] of superconducting niobium, it was found that the μ^+ is rapidly diffusing even at very low temperatures. Diffusion in

ferromagnetic iron and nickel[27] has also been studied, as will be described in a later section. The determination of the μ^+ site in a metallic host has not yet been performed, but studies of ferromagnetic metals may make this possible.

C. μSR in Ferromagnets

Metallic ferromagnets are fascinating systems to study with μSR. There is at present much interest[28-31] in impurity states in these materials, and the μSR technique is very well adapted to just this sort of investigation.

One of the earliest investigations of ferromagnets with muons was an experiment[32] by Rasetti in 1944. Using cosmic ray muons and with a counting rate of one per hour, he set out to find if muons passing through magnetized iron feel the magnetic field B or H. In an interpretation of this data, Wannier[33] stressed the importance of the "interpenetration of the muon and the magnetized electrons". In more modern terminology, this interpenetration is the source of the Fermi contact interaction.

In 1971 an attempt[34] was made at the Lawrence Berkeley Laboratory to observe μ^+ precession in a spherical collection of iron filings. The large variety of demagnetizing fields produced a large internal field inhomogeniety, and rapid depolarization prevented the observation of precession.

A group headed by W. J. Kossler at The College of William and Mary first observed[35-37] coherent μ^+ precession in a ferromagnet in 1972. They studied polycrystalline samples of Ni and Fe at room temperature and above. In a collaboration with a group from Bell Laboratories, they later extended their studies[38] to the ferromagnets dysprosium and gadolinium.

After the initial work by Kossler, et. al. our group at LBL observed precession[39] in a saturated sample of polycrystalline Ni and at low temperature (77K) in a single crystal of Ni, and

we theoretically interpreted[40] the observed contact field. Experiments were also done[41] in Ni at temperatures near the Curie point, and room temperature precession was observed in a single crystal of iron.

A group at Dubna in the USSR has performed experiments[42] on polycrystalline Ni, Fe, and Co, focusing attention[27] on the temperature dependence of the depolarization in Fe and Ni at lower temperatures and on the sign of the local field in these materials[43]. A theoretical paper on μ^+ in ferromagnets[44] has been published by Ivanter.

Our assumption that the positive muon occupies an interstitial site in Ni and Fe is at present based on circumstantial evidence. A positive muon in matter is electronically almost identical to a proton. Neutron diffraction experiments on $Ni\text{-}H_{.6}$ have demonstrated[19] that the protons occupy octahedral interstitial sites in the fcc Ni lattice. Although the hydride is far from the dilute limit of the μ^+ technique, we are prompted to explore the consequences of our assumption. The locations of the tetrahedral and octahedral sites in the fcc unit cell are shown in Figure 1.

In a metal, the correct description of the electronic state of the μ^+ is a bare muon surrounded by a screening cloud of unbound conduction electrons. The fact that the μ^+ binds an electron, forming muonium[4], in insulators suggests the intriguing possibility of observing coherent interstitial muonium precession in insulating ferromagnets or antiferromagnets.

In a ferromagnet like Fe or Ni, the muon's electronic

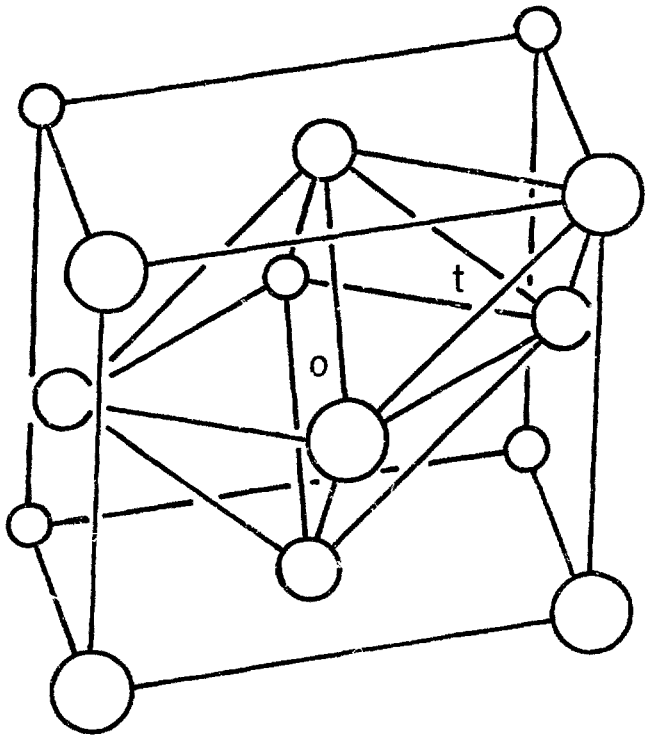

XBL 753-646

Figure 1. The unit cell of Ni (fcc) showing the positions of the octahedral (o) and tetrahedral (t) interstitial sites. To aid in visualization, the 6 octahedral and 4 tetrahedral nearest Ni neighbors have been joined by lines.

screening cloud is polarized to some extent. This polarization produces[45] an isotropic contact or hyperfine field at the muon which is proportional to the degree of polarization and to the electron density at the μ^+.

There is also a classical dipolar interaction between the μ^+ and the localized polarized electrons on the neighboring cores of its host. Furthermore, this classical dipolar interaction may appear enhanced if the contact interaction mentioned above has not only an isotropic part but a part with dipolar symmetry as well. Such an effect is known as pseudo-dipolar enhancement[46] and is a result of an aspherical charge or spin distribution in the muon's screening cloud.

All dipolar fields vanish at a site with cubic symmetry in the ordered phase. This applied to both the octahedral and tetrahedral interstitial sites in fcc Ni. Here, the only field the μ^+ sees is the isotropic contact field.

The situation is radically different in bcc iron where the face-centered interstitial sites do not have cubic symmetry. The dipolar fields are substantial here.

Cobalt, with the hcp structure, is an intermediate case. If the c/a ratio were perfect, the interstitial sites would have cubic symmetry, for nearest neighbors. In reality, c/a for cobalt differs by 1% from the perfect value implying that small dipolar fields exist at the interstitial sites in addition to the isotropic contact field.

The elegant cancellation of dipolar fields in ferromagnetic Ni no longer occurs when the cubic symmetry of the muon site

is destroyed, as it is above the Curie temperature or in a deformed or impure crystal. In controlled experiments of these sorts, the dipolar fields can be made visible and studied.

It would be of great value to determine the state of motion of the μ^+ in the ferromagnets under study. Besides being of intrinsic interest, the state of motion determines much about how the μ^+ samples the host's magnetism.

An extrapolation of permeation time lag measurements[47] indicates that protons in nickel below about 200K are stationary on the time scale of our experiment, undergoing only zero point oscillations about the equilibrium position at the center of the octahedral interstitial site.

Positrons diffuse much more rapidly due to their low mass. Calculations for various metallic hosts[48] suggest an increase in diffusion rate of about 10^9 over protons.

The μ^+, with a mass between that of the proton and positron, may be at rest or in rapid motion; an experimental investigation is called for. The experiment[25] performed on muons in Cu mentioned earlier suggests an elegant way to study the motion of μ^+ in ferromagnets. In copper, the nuclear moments of the host present the muon with a microscopically inhomogeneous magnetic field. The diffusion of the μ^+ narrows this linewidth. If different μ^+ sites in Ni can be made magnetically inequivalent, μ^+ motion in Ni can be studied in a similar manner.

One method of introducing microscopic inhomogeniety is to alloy the Ni with another element. The solute will in general not have the same electronic moment, and a dilute random

distribution of these impurity atoms will produce the desired field inhomogeniety. A preliminary investigation of Ni-V alloys by our group yielded inconclusive results.

The artificial introduction of field inhomogenieties would be unnecessary if the μ^+ sampled both the tetrahedral and octahedral interstitial sites in the Ni fcc lattice. Although the dipolar field in both of these sites is zero, they presumably have different hyperfine fields. It was hoped that one could study the temperature dependent jump rate of the μ^+ among these inequivalent sites. It is known[27] that no dramatic changes in the muon precession occur down to temperatures of 100K. We performed an experiment in which a single crystal Ni sample was cooled to 0.12K. It was hoped that two precession components would be visible corresponding to muons frozen in the two types of site.

Only one precession component was seen at this low temperature, and the frequency was just a simple extrapolation of the earlier results at higher temperature. This implies that either the μ^+ samples only one type of site at all temperatures, or that it is moving rapidly (quantum tunneling) even at 0.12K.

Because iron is bcc, and because the easy axis is [100], well below saturation, it has two electrostatically equivalent interstitial sites (on the cube faces) which have radically different dipolar fields. The magnitude of the dipolar field at one site is twice that at the other, but the low field site is twice as common. Since the fields at the two sites have opposite signs, rapid muon motion will average out their

contribution. Thus, the expected precession pattern in iron at high temperature is a single long-lived component.

The effect of decreasing the μ^+ jump rate will be first to shorten[7] the relaxation time of the precession (as the jump rate becomes equal to the precession frequency difference). Just such a dramatic drop in relaxation time has been observed for muons in polycrystalline ferromagnetic iron[27].

If the sample is a single crystal of iron, and if at low temperatures muons become frozen in the two inequivalent sites, long-lived precession at two different frequencies should be observed[7]. Preliminary experiments by our group on a small iron crystal at 77K were inconclusive.

D. Organization of the Dissertation

This dissertation is divided into three main parts. The first describes the μSR technique as applied to a general sample. Topics include the production, stopping, and decay of the μ^+, a description of the experimental set-up and counting procedure, and a description of the methods of data analysis.

The second part presents experimental and theoretical work done with μSR in Ni in the ferromagnetic state, far below the Curie temperature. The local field at the μ^+, including its temperature and field dependence, is discussed. Differences between single crystal and polycrystalline samples are stressed and a theoretical treatment of the hyperfine field is presented.

In the third part, work done on Ni near the Curie temperature is described. This includes a determination of the critical exponent β and an experimental and theoretical treatment of the observation of critical spin fluctuations with μSR.

II. EXPERIMENTAL DETAILS

A. Medium Energy Physics

At this point a brief description of how our positive muons are produced, are brought to rest in the sample, and end their life is in order. This description will be sketchy on purpose as the details have been presented in [1,2] other publications.

The process begins when the external proton beam of the 184" Cyclotron of LBL strikes a copper pion production target. Only a part of the beam strikes the target, allowing for the simultaneous operation of a second experiment downstream. Out of the multitude of nuclear interactions which occur in the copper comes a substantial flux of positive pions. Those with the correct momentum enter the muon channel which is composed of a bending magnet followed by two quadrupole focusing magnets and a second bending magnet. The first bend selects pions of a definite momentum. These pions then decay during their flight through the channel into positive muons and unseen neutrinos. Because the decay occurs in flight and because it is an example of a non-parity conserving weak interaction, a μ^+ beam with two oppositely polarized components results. The higher energy or "forward" muons are the ones used in our experiment. These are polarized anti-parallel to their momentum direction. The last bend serves to separate these forward muons from the backward muons and the undecayed pions. The forward muons have a kinetic energy $E_{ke}^{\mu} = 150$ MeV at this point.

The μ^+ beam then passes through a 2" copper degrader which further eliminates the pion component and slows the muons from 150 Mev to 30 Mev such that they stop in the sample under study. A metal sample of typical size is 3" by 2" in area and 1/2" thick and stops about 1500 muons per second.

The stopping of the μ^+ in liquids and gases (the case of insulators should be fairly similar) has been described earlier[1]. The case of metallic samples, which are of prime interest in this dissertation, deserves special mention. As in liquids and gases, the energy loss during the beginning of the stopping process is purely due to ionization of the host atoms by the bare muon. This mechanism dominates until the μ^+ velocity drops to typical electron velocities in the sample (v_F, the Fermi velocity, for conduction electrons and αc for core electrons, both of which are about 2×10^8 cm/sec) at which point $E_{ke}^{\mu} \approx 3$ Kev. The capture of an electron by the muon now becomes possible. A rapid succession of electron captures and losses follows until the velocity drops to the point where very little energy is lost per collision and a state of quasi-equilibrium is reached with the μ^+ holding on to one electron. Inelastic collisions of this muonium atom with the host atoms slows the muon further until the collision frequency drops below the response frequency of the conduction electrons. Below this response frequency (i.e. the plasma frequency $\sim 5 \times 10^{14}$ sec^{-1}) a screening cloud forms around the μ^+ and a bound state no longer exists. This ionization occurs at an energy $E_{ke}^{\mu} = 15$ ev. The μ^+ continues to drop to thermal energies as a bare muon plus a screening cloud. The

problem of μ^+ stopping in metals has been treated from another point of view by Smirnov[49].

The question now arises: what happens to the muon polarization during this catastrophic slowing down. The only interaction which can reorient the μ^+ spin is a magnetic interaction. Since the entire stopping process takes less than 10^{-9} sec, the muon would have to feel an average field of 10^4 gauss in order to precess one radian during its stop. In order to become depolarized, the ensemble of stopping muons must see a field distribution whose width, after being averaged over the path of a stopping μ^+, is 10^4 gauss. This criterion cannot be met even in magnetized ferromagnets. It is true, however, that fields of 10^5 gauss are produced at the μ^+ by a bound electron, but the upper limit for an estimate of the time during which the stopping μ^+ binds an electron is 10^{-12} sec, which again precludes depolarization. Indeed, it is found experimentally that little or no polarization is lost when the muon stops in metallic ferromagnets.

The stopping μ^+ certainly causes a significant amount of radiation damage (vacancies, dislocations, voids, etc). Since the highest density of this damage occurs at the end of the muon's range, an important question is whether the μ^+ subsequently interacts with the damage caused by its own stop. There is alot of uncertainty about this question, and each material should be examined separately. In this dissertation, it will be assumed that the μ^+ diffuses away from the stopping damage, sampling only pure, undamaged material. This assumption requires further verification.

We now have a thermalized, polarized μ^+ in the sample. During its 2.2 μsec lifetime, magnetic interactions reorient the μ^+ spin either coherently, resulting in spin precession, or incoherently, resulting in depolarization. The nature of these magnetic interactions forms the bulk of this dissertation.

The μ^+ decays according the the scheme: $\mu^+ \rightarrow e^+ + \nu_e + \bar{\nu}_\mu$ where the only observed product is the positron. Like the pion decay, this is an example of a non-parity conserving weak interaction. It is found that the angular distribution of the decay positrons is asymmetric, having the form[2] $f(\theta) = 1 + 1/3 \cos(\theta)$ after averaging over the positron energy. Here θ is the angle between the μ^+ spin and the positron momentum. It is the higher energy positrons that are emitted in the forward direction, so if one selects according to positron energy (at the expense of counting rate), the asymmetry of the distribution increases. Since very low energy positrons fail to leave the sample, we automatically perform some degree of energy selection. The maximum positron energy corresponds to a range in copper of 2 cm.

B. Experimental Technique

A simplified sketch of the sample and counter geometry is presented in Figure 2. For further details, the reader is referred to Reference 1. The detection of the incoming muons and exiting positrons is performed by two counter telescopes (drawn schematically as the two counters A and B in the figure), one in front of and one behind the target. The counters are plastic scintillators optically coupled to photomultiplier tubes. Pulses from the tubes are fed into several banks of electronic logic that determine when specified coincidences occur.

A muon which stops in the sample registers a count in the forward or A counter with no corresponding count in the backward or B counter. The $A\bar{B}$ coincidence defines the time t_1 and starts a very fast clock. At this time the μ^+ polarization is known to be pointing back toward the A counter. The muon then decays with a mean lifetime of 2.2 μsec. Approximately 2% of the decay positrons from stopped muons leave the sample and pass through the B counter, giving no corresponding count in the A counter. This $\bar{A}B$ coincidence defines the time t_2 and stops the fast clock. It is the time difference $\Delta t = t_2 - t_1$ which is of interest, and an experimental run consists of $\sim 10^6$ measurements of this quantity.

A histogram of the number of occurances of the measured values of Δt will have the general shape of a simple exponential decay corresponding to the 2.2 μsec decay of the μ^+. But if the μ^+ is precessing in the external field or some internal field, the precessing anisotropic angular distribution of the emitted positrons will cause the average counting rate of the B counter

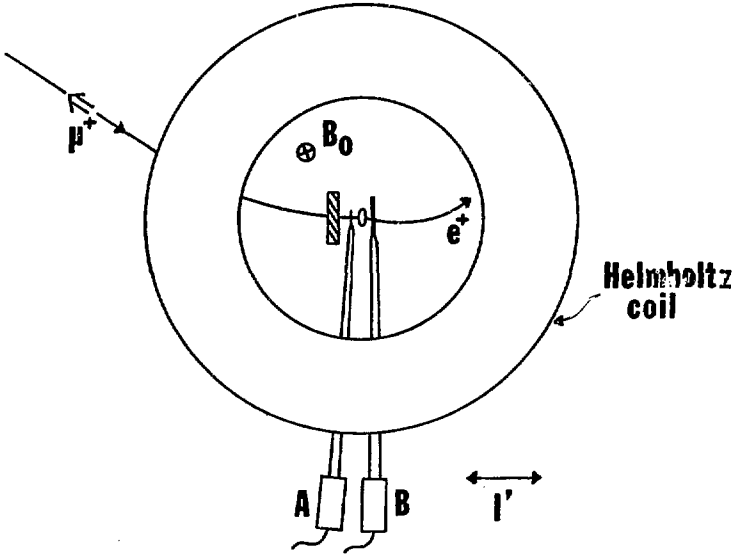

XBL 753-702

Figure 2. A simplified view of the experimental set-up showing the precession coils, degrader, and target. The two counters A and B are in reality two sets of several counters each.

to vary cyclically with Δt, and the histogram will have a sinusoidally oscillating component superimposed on the exponential envelope. The frequency of these oscillations is identical to the Larmor frequency of the precessing muon. A typical histogram is shown in Figure 3.

The heart of the electronic logic is the fast clock. We use a Hewlett-Packard type 5360A Computing Counter which has a time resolution of 0.1 nsec. The time intervals measured are binned into 0.5 nsec bins and the overall time resolution of the system (including the counters, coincidence logic and clock) is about 1 nsec. This places a limit of 1000 MHz on the highest precession frequency we can observe. The digitized time intervals from the clock go to an on-line Digital Equipment Corporation PDP-15 computer where the histogram is stored and updated.

The PDP-15 is also capable of doing limited data analysis such as a Fast Fourier Transform[50] during an experimental run. For archival storage and for input to the larger computers at LBL the final histogram is written on magnetic tape at the conclusion of each run. A histogram consists of 12,000 bins corresponding to 6 μsec or about 3 muon lifetimes. Just as the time resolution limits the highest frequency we can observe, the histogram length (which is dictated by the muon lifetime) sets a lower limit of about .15 MHz on the accessible frequency range.

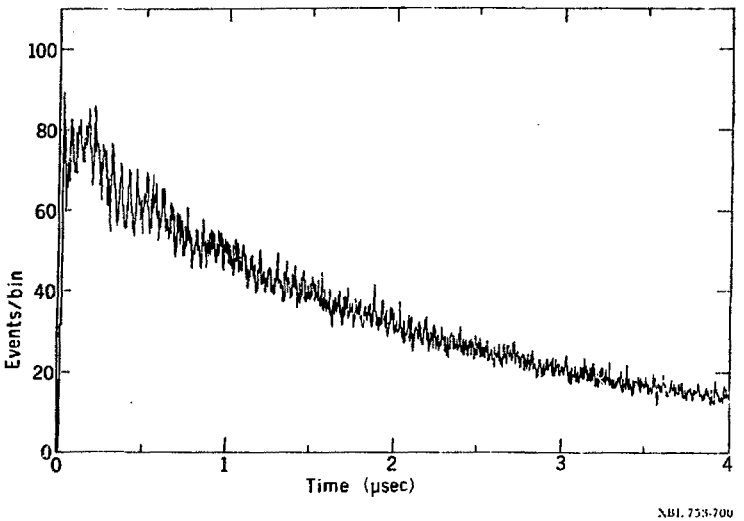

Figure 3. An experimental histogram taken for a single crystal of Ni in a refrigerator at 20 K and in an external field of 150 gauss.

Counting rates for a metallic sample of typical size (3" x 2" x 1/2") are as follows:

Incident muons	3000/sec
Stopped muons	1500/sec
Detected positrons ("good" events)	30/sec
"Bad" events	3/sec

A "bad" event is defined as one in which the succession of pulses made the interpretation of the event ambiguous. This would be the case, for example, if two muon stops occurred in rapid succession before a positron was detected or the clock was reset. Bad events were discarded by the logic. Note that with this μ^+ stopping rate and a 2 μsec μ^+ lifetime, we can be fairly sure of having only one muon at a time in our sample.

We often found it desirable to apply an external magnetic field to the sample. This was accomplished with a large set of Helmholtz coils. Helmholtz coils have the advantage of providing easier access to the sample than a pole tip magnet. In addition, the use of Helmholtz coils avoids the problem of field inhomogeniety from the magnetic image charges induced on the pole tips by a magnetic sample.

The coils used in our experiment were adjusted to give fields from 4.4 kG to 15 G with an inhomogeniety across the sample of less than 0.3 G. The fields were not regulated directly but the drift in the supply current was less than 0.1 percent.

The samples could be cooled or heated through the temperature range 0.1 K to 1000 K using refrigerators and ovens to be described later in the text.

C. Data Analysis

The general mathematical form of the histogram is:

$$F(t) = N_o \{B + e^{-t/\tau_\mu} [1 + \sum_{i=1}^{n} A_i e^{-t/T_2^i} \cos(\omega_i t + \phi_i)]\}$$

for n different precession components (corresponding for example to n different muon stopping sites in a ferromagnet). Here N_o is a normalization factor proportional to the number of events taken, B is the time independent accidental contribution, τ_μ is the muon decay time (2.2 μsec) and A_i, T_2^i, ω_i and ϕ_i are respectively the asymmetry, relaxation time, angular frequency and initial phase of the i^{th} precession component. In extraordinary cases (such as precession in the presence of a large static field inhomogeniety) the relaxation expression e^{-t/T_2} must be replaced by a gaussian decay e^{-t^2/T_2^2} or something intermediate between an exponential and a gaussian. The experimental histogram differs from this ideal form due to statistical variations in the population of each bin. The average of a large ensemble of histograms collected under identical conditions is described by the mathematical form given.

The parameters of interest in the present experiments are A_i, ω_i and T_2^i. The easiest way of finding A_i and ω_i as well as identifying how many different frequency components there are is to do a discrete Fast Fourier Transform[50] of the experimental histogram using for example the CDC 7600 computer of LBL. In general this procedure is preceded by division by N_o, subtraction of the background contribution and multiplication by

e^{+t/τ_μ}. Transforms of 1024 to 8192 points were routinely performed quickly and inexpensively. A typical transform is shown in Figure 4. Ideally, one can get a value for T_2^i from the width of the i^{th} Fourier transform peak, but this was found to be grossly inadequate due to the discrete nature of the transform. A better technique, and one that is also fairly inexpensive, involves performing a series of Fast Fourier Transforms, each over a successively later part of the data. The area under the Fourier transform peak of interest is then plotted against the time window shift. In this way the relaxation may be seen directly. This technique is especially valuable when many components of small asymmetry are present simultaneously in the data.

When only a few (one or two) large components are involved, a multi-parameter non-linear fit to the data may be performed. The fitting procedure we used was the Maximum Likelihood Method[51], and typically 7 to 9 parameters were fit simultaneously. Often the amount of computing involved in such a fit could be substantially reduced by condensing the histogram into a smaller number of bins. An advantage of using the fitting procedure is that a realistic estimate of the errors in the fitted values of the parameters can be computed by the fitting program.

The statistical uncertainties in the experimental histogram are of course reflected in noise peaks in the Fourier transform and uncertainties in the fitted values of the parameters. An account of the Fourier transform and fitting data reduction techniques and a description of the statistical errors involved are presented in the Appendix.

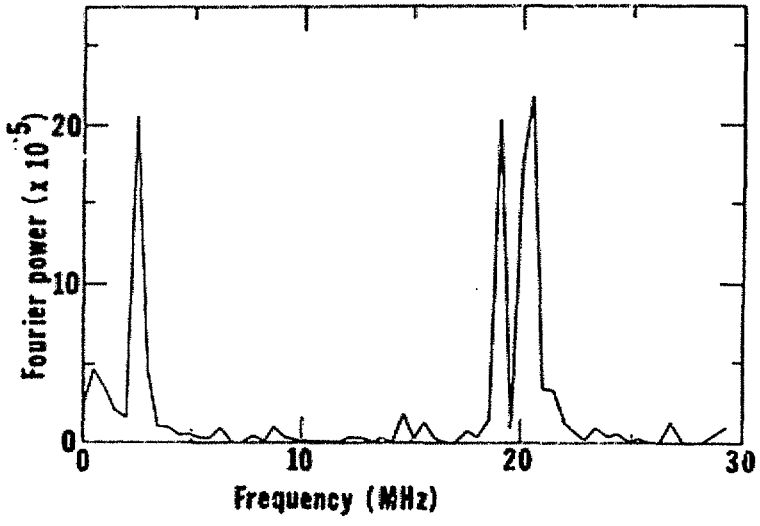

XBL 755-704

Figure 4. A Fourier transform of the experimental histogram shown in Fig. 3. The three strong components are, in order of increasing frequency, the 150 gauss μ^+ component from the walls of the refrigerator, a 19 MHz background signal from the time structure of the cyclotron beam, and the 1.5 kG μ^+ component from the Ni crystal.

III. μSR in Ni; $T \ll T_C$

A. Theory

1. The Local Field B_μ

A measurement of the precession frequency of the μ^+ in Ni is equivalent to a measurment of B_μ, the local field at the μ^+.

B_μ is composed of the following contributions:

$$B_\mu = B_o - NM + \frac{4\pi M_s}{3} + B_d + B_{hf}.$$

B_o is the externally applied field, M is the bulk magnetization of the sample (macroscopically uniform in an ellipsoidal sample), M_s is the saturation magnetization, $\frac{4\pi M_s}{3}$ is the "Lorentz field" from magnetic charges on the surface of a small hypothetical spherical cavity centered on the μ^+ within a domain, B_d is the dipolar field from Ni cores within the Lorentz sphere, and B_{hf} is the hyperfine field seen by the muon due to its isotropic contact interaction with polarized screening electrons.

$B_o - NM$ is just H_{in}, the internal H field. Below saturation, H_{in} cannot be greater than the coercive force (about 2 gauss), and we can ignore this contribution to B_μ. If one assumes that the muon is situated at a site with cubic symmetry (i.e., the tetrahedral or octahedral interstitial site), the dipolar fields of Ni cores within the Lorentz sphere will be zero. Thus, below saturation, we have the relation:

$$B_\mu \simeq \frac{4\pi M_s}{3} + B_{hf}.$$

2. Screening of Positive Impurities in Metals

Because the materials of interest in this dissertation are metals, and because the hyperfine field depends strongly on the electronic structure of the impurity state, a discussion of the screening of a positive impurity in metals is in order. The special features that arise in the metallic state are due to the presence of free or nearly free conduction electrons.

A positive impurity (such as a μ^+ or a proton) attracts neighboring conduction electrons; it surrounds itself with a screening cloud. This configuration represents a new electronic energy state not present in the pure metal. The nature of such an impurity state has been the subject of a large amount of theoretical study.[5,28,45,52-55]

An important question arises immediately: does the impurity-screening cloud system resemble a hydrogen atom, in which a single electron can be said to be bound to the impurity, or is the screening cloud merely a localized region of higher density in the electron gas where mobile electrons temporarily congregate. In the first case we have a bound state; in the second case, we have what Friedel[56] calls a "virtual bound state".

It may at first seem that the difference between a bound and a virtual bound state is only a quantitative one regarding what the average "occupation time" of an electron on the impurity is. However, a rigorous criterion exists which can be used to decide between the two states: does a bound state exist in the screened potential of the impurity[5]. Or alternatively one can ask: what is the position of the newly formed impurity state with respect

to the electronic energy bands of the bulk material.

Koster and Slater[55] have performed a theoretical calculation of the position of such an impurity level as a function of the strength of the impurity potential. They found that for a weak potential, the new level falls within an energy band of the bulk material and that the scattering of band electrons by the impurity is significant for electrons whose energy is close to the impurity level. This is Friedel's virtual bound state.

Friedel introduced the concept of a virtual bound state from phenomenological considerations[56] and described it as follows: since the impurity state occurs in the band, it has the same energy as some extended or band state. This allows the impurity state to resonate with the band state, increasing its amplitude. The enhanced band state in turn resonates with other band states of nearly the same energy, passing on some of its enhanced amplitude. The process is repeated again and again with the net result of a broadening of the impurity state in both space and energy. Since a well-defined electronic state can no longer be associated with the impurity, the original state is said to have become a virtual state.

As Koster and Slater's impurity potential is increased, a critical value is reached at which the impurity state leaves the bottom of the band. Impurity state-band state resonance is now no longer possible, and the impurity state retains a discrete energy. A bonafide bound state now exists with a single electron associated with the impurity.

In metals for which the free-electron gas model is a good approximation (e.g., the alkalai metals), a singly-charged positive impurity forms a virtual bound state[5]. The situation is more complicated in non-free-electron gas metals such as the transition metals and the rare earths[28]. The position of various partially localized energy bands (such as the 3d-bands in Ni) with respect to the Fermi level is an important factor in determining the nature of the screening cloud.

There is strong evidence that hydrogen gives up its electron when it enters some of the transition metals. As hydrogen is dissolved in Ni or Pd the paramagnetism of the host decreases[57,58] until it vanishes at a critical hydrogen concentration. This effect has been interpreted as a filling of the holes in the host d-band with electrons contributed by the hydrogen.

In a few transition and rare earth metals, absorbed hydrogen forms a covalent bond with a host atom[15,52]. In this case, a discrete impurity energy state is established with the formation of a molecular bound state.

It is of interest to calculate the electron density n(o) at a positive impurity in a free electron gas of density n_o. We assume that the screening may be treated as a linear response, allowing us to use the following expression[59]:

$$n(o) = n_o + \frac{1}{(2\pi)^3} \int d^3q \left(1 - \frac{1}{\varepsilon(o,\vec{q})} \right)$$

where $\varepsilon(o,\vec{q})$ is the zero frequency, momentum dependent dielectric function. The simple Fermi-Thomas approximation[59]

for ϵ:

$$\epsilon_{FT}(o,\vec{q}) = 1 + \frac{1}{r_s^2 q^2}$$

gives an infinite value for n(o) and is thus unacceptable. $r_s = (E_F/6\pi n_o e^2)^{1/2}$ is the Fermi-Thomas screening length, and E_F is the Fermi energy. A better approximation[60] is the Lindhard self-consistent field dielectric function:

$$\epsilon_L(o,\vec{q}) = 1 + \frac{1}{2q^2 r_s^2}\left\{1 + \left(\frac{k_F}{q} - \frac{q}{4k_F}\right) \ln\left|\frac{2 + \frac{q}{k_F}}{2 - \frac{q}{k_F}}\right|\right\}$$

where k_F is the Fermi momentum. Both r_s and k_F are functions only of n_o. After a simple numerical integration, we obtain the curve plotted in Figure 5.

Also plotted are the results of a calculation by Pathak[53] which includes the effect of electron-electron interactions. Both of these calculations of n(o) are done in the linear response approximation. A self-consistent calculation[54] which accounts for non-linear contributions indicates that these corrections may substantially increase n(o).

3. The Hyperfine Field in Ni

As we have seen, the elegant cancellation of the interstitial dipolar fields in nickel simplifies the interpretation of B_μ, the local field. The important measured quantity is B_{hf}, the hyperfine field seen by the μ^+ due to its Fermi contact interaction with the polarized screening electrons.

In this section, a very simple calculation of the hyperfine

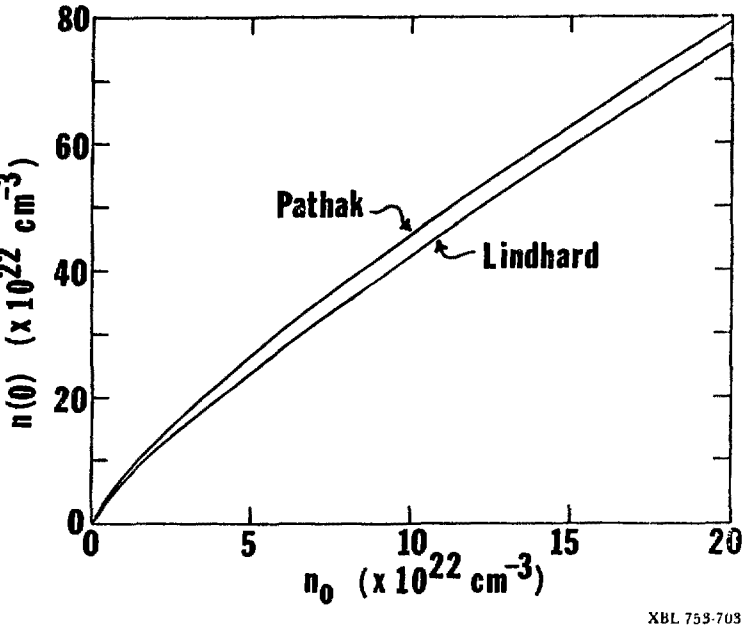

XBL 753-703

Figure 5. The calculated relation between n_o (the μ^+-absent charge density) and n(o) (the density at the μ^+). Both curves are for a free-electron gas in the linear response approximation, but Pathak's calculation includes the effect of electron-electron interactions. It has been suggested[54] that both of these calculations underestimate n(o).

field is performed. To date, two other theoretical treatments of this type of problem have been published.

Ivanter has published a paper[44] discussing the hyperfine field of the μ^+ in a ferromagnet in which it is assumed that muonium is formed. The μ^+ exchanges its bound electron with the surrounding bath of polarized electrons. He predicts no hyperfine field for the unbound state. Although this is perhaps the best approach for treating ferromagnetic insulators, it is not applicable to ferromagnetic metals where no bound state exists.

Stearns has treated the case of μ^+ in iron[61]. In this investigation, she effectively extrapolates the hyperfine field at the nucleus of an interstitial iron atom in iron from the measured hyperfine field at the interstitial μ^+ in iron. This interstitial iron result is then interpreted in terms of a "conduction electron polarization curve".

In our treatment of the μ^+ in Ni, we will assume that the muon is located in the octahedral site in the fcc Ni lattice (although only minor changes would result from a switch to the tetrahedral site) and that no bound state is formed.

The treatment begins with the expression for the Knight shift[46];

$$\Delta B = \frac{8\pi}{3} \chi_s B_o \langle |u_K(o)|^2 \rangle_{E_F} .$$

Here, ΔB is the field seen by a magnetic probe in a metal due to its hyperfine interaction with conduction electrons polarized by the external field B_o. The quantity in brackets is an average over the periodic part of the conduction electron Bloch functions.

We will work in the free electron model where $u_k = 1$. χ_s is the spin susceptability. The product $\chi_s B_o$ may be written as the local magnetization m_{loc}:

$$B_o \chi_s = m_{loc} = -\mu_B [n^{\uparrow}(o) - n^{\downarrow}(o)].$$

μ_B is the Bohr magneton, and $n^{\uparrow}(o)$ and $n^{\downarrow}(o)$ are the densities of spin up and spin down electrons at the site of the μ^+. We then assume that instead of an external field, some other agent produces a non-zero local magnetization. ΔB in this case becomes the hyperfine field produced by the local magnetization:

$$B_{hf} = -\frac{8\pi}{3} \mu_B [n^{\uparrow}(o) - n^{\downarrow}(o)] .$$

This is the expression derived by Daniel and Friedel[45]. It proves convenient to define the conduction electron polarization at the μ^+,

$$\zeta(o) = \frac{[n^{\uparrow}(o) - n^{\downarrow}(o)]}{n(o)}$$

where $n(o) = n^{\uparrow}(o) + n^{\downarrow}(o)$. The hyperfine field may then be written:

$$B_{hf} = -\frac{8\pi}{3} \mu_B \zeta(o) n(o) .$$

Using neutron diffraction, Mook[62] found that the unperturbed or "muon absent" moment density at the octahedral interstitial site in ferromagnetic Ni is:

$$-\mu_B [n_o^{\uparrow} - n_o^{\downarrow}] = -\mu_B \zeta_o n_o = -0.85 \times 10^{22} \mu_B/cm^3 = -0.079 \text{ kG}.$$

Our first model is a "very naive" picture in which no screening of the muon's charge occurs. Then $n^{\uparrow\downarrow}(o) = n_o^{\uparrow\downarrow}$,

giving $B_{hf} = \frac{8\pi}{3}$ x (-0.079) kG or B_{hf} =-0.66 kG. We anticipate that the effect of screening will be important and as a first attempt to improve this estimate, we could assume that ζ is independent of charge density. Thus the predicted hyperfine field would be enhanced by the factor $n(o)/n_o$ (see Figure 5). To proceed further, information about the conduction electrons in Ni is needed. We defer further discussion until after the experimental data is presented.

B. Experimental Results

1. Samples, Ovens and Refrigerators

The study of Ni in the ferromagnetic state represents a major part of this dissertation, and I turn now to the presentation of our experimental results.

Both polycrystalline and single crystal samples of Ni were used in our investigations. The polycrystalline sample was made from a plate of 99.6% Ni purchased from Pacific Metals in San Francisco, California. It was made in the shape of an ellipsoid in order to produce a uniform internal magnetization. The sample was thin along the beam direction to allow the decay positrons to escape through to the positron telescope. Also, a large cross sectional area was presented to the beam to maximize the counting rate. Finally, since we wanted to study the effects of different demagnetizing fields, an ellipsoid with three different principal axes was chosen. The plate was sawed, milled, and finally sanded to this shape -- 1/2" x 2" x 4 1/2". The 1/2" axis was always oriented along the beam direction, and either the 2" or the 4 1/2" axis was oriented along the externally applied magnetic field. The sample was not annealed.

Several single crystal Ni samples were used in the course of our experiments. A roughly spherical crystal (1" diameter) of unknown source and a purity of 99.995% was used in the initial experiments at room temperature and at 77K. Counting rate considerations dictated that a larger crystal was needed.

A very large single crystal of Ni was purchased from Atomergic Chemicals Co., Long Island, New York. This crystal

also had a purity of 99.995% and had many twins with a mosaic spread of about 2 degrees. The crystal was cut into many pieces, the largest of which was a rough ellipsoid of dimensions 1/2" x 2" x 6". This piece was spark cut from the original crystal and was not machined at all. This piece was used for refined experiments at room temperature and 77K. A rectangular prism was also cut from the large crystal. The two largest cuts were spark cut, and the four smaller cuts were cut on a mechanical hacksaw. The final dimensions of the prism were 1/2" x 1 1/2" x 2 1/2"; this sample was used in an experiment at 20K and an experiment near the Curie temperature. A second rectangular prism was cut in the same manner from the large crystal, and this one was then shaped by sanding to an ellipsoid of dimensions 1/2" x 1 1/2" x 2 1/2". This sample was used in experiments at 0.12, 1, 4, 77K, room temperature, and close to the Curie temperature. All the single crystal samples had the [111] crystalline axis (the easy axis of magnetization) along the long dimension.

Experiments were performed at many temperatures, both above and below room temperature. Heating and cooling devices of varying degrees of sophistication were constructed for these investigations. The ovens which were used for runs near the Curie temperature will be described in a later section.

Two series of runs were done with the polycrystalline sample at 250 and 300 degrees C. A layer of asbestos tape was wrapped around the ellipsoid on which a non-inductive winding of nichrome heater wire was wrapped followed by a second layer of

asbestos tape. A chromel-alumel thermocouple was firmly attached to the center of the sample and used to monitor the temperature. No automatic regulation of the temperature was performed and the drift with time was perhaps 20 degrees.

Experiments at 77K utilized a stryofoam dewar containing liquid nitrogen. The sample was situated in the bottom of the dewar and the surrounding region in the beam was packed loosely with styrofoam to minimize μ^+ stops in the nitrogen. The dewar was filled automatically.

For runs at 20K, the sample was bolted to a copper cold finger attached to a Cryomech refrigerator. The temperature was monitored with a carbon resistor.

A dilution refrigerator was used for runs at 4, 1, and 0.12 K. This appratus was hand made by our Japanese colleagues. At 4K, the sample was immersed in liquid helium, and at the lower temperatures, it was in thermal contact with various cold walls of the refrigerator. The temperature was monitored with a germanium resistor.

In all the hot and cold runs, a significant fraction of the muons stopped in the cryostat walls or heater wrappings. This posed no problem for studies of the ferromagnetic phase, because as will shortly be described, muons stopped in the ferromagnetic Ni see a magnetic field quite different from the applied magnetic field. Fourier transforms of the data show two well separated components, one from the walls and one from the Ni (see Figure 4). However, the walls were kept as thin as possible to maximize the muon stopping rate in the Ni sample.

2. B_μ and The Effect of External Field and Temperature

After the first report of coherent μ^+ precession in a heated polycrystalline Ni sample below saturation[35], we undertook a study of the effect of an externally applied magnetic field on the precession frequency in a heated polycrystalline ferromagnetic Ni sample. Muons were stopped in the polycrystalline ellipsoid described above at two temperatures with the sample in two orientations with respect to the external field. Various fields were applied for each of the temperature-orientation combinations.

We found, in agreement with Kossler's group, that below saturation the local field seen by the muon (B_μ) is independent of external field (Figure 6). The two orientations of the sample, "Horizontal" and "Vertical" (2" or 4 1/2" axis parallel to the field), presented two different demagnetization factors, N_v and N_h, and hence, two different (temperature dependent) saturation fields. The calculated[63] values of N_v and N_h are 0.688 and 2.24 respectively. As the external field was raised above the saturation field of the sample, the local field began to increase linearly with the excess over the saturation field (Figure 6). This is the expected result; below saturation, magnetic shielding prevents the external field from penetrating the sample. After the domain walls have moved to their limiting positions, the saturation is complete and no further shielding is possible. The excess field leaks into the sample.

This type of experiment provides a very clear answer as to the sign of the local field. If, above saturation, the local field initially increases, as in the case of nickel, B_μ is positive. It

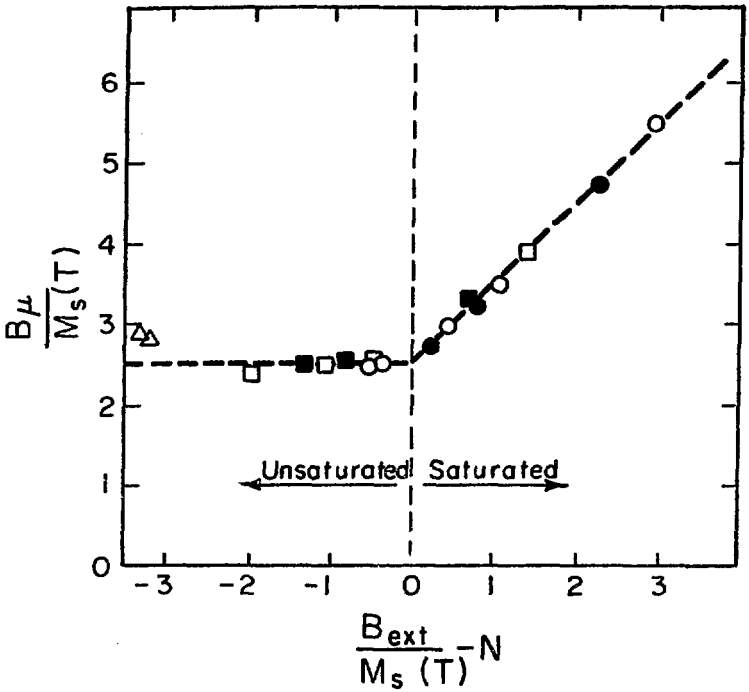

XBL7310-4386

Figure 6. The local field at the muon site in nickel vs. B_{ext}, the external field measured with target out. N is the sample demagnetizing factor. The points denoted by triangles are from data on an approximately spherical single crystal with the [111] axis parallel to B_{ext} at 300 and 77 K. Other points are from data on a polycrystalline ellipsoid (4.5"x2"x0.5"). Solid and open circles refer to the 4.5" axis parallel to B_{ext} (N = 0.688) at 250 and 300 C respectively. Solid and open squares refer to the 2" axis parallel to B_{ext} (N = 2.24) at 250 and 300 C. The fields B_μ and B_{ext} have been normalized to bring measurements at various temperatures to the same vertical level and to exhibit saturation for all samples at zero on the horizontal scale.

has recently been determined[43] by this type of investigation that B_μ in iron is negative. Here the magnitude of B_μ decreases just above saturation until it reaches zero, at which point it begins to increase again.

The temperature dependence of B_μ is shown in Figure 7. The local field remains roughly proportional[64] to $M_s(T)$ throughout the temperature range studied (0.12 K to T_c).

The measured value of B_μ at 77 K is + 1.48 kG. The Lorentz field at low temperature is + 2.14 kG, which implies a value for B_{hf} of -0.66 kG. Notice that this is in perfect agreement with the "very naive" no-screening picture. We are now faced with the problem of accounting for this agreement in the presence of the substantial screening which must occur.

If one attempts to extract values[37] of B_{hf} for higher temperatures, one finds a complicated temperature dependence for the case of an unsaturated polycrystalline sample. B_{hf} begins to decrease as the temperature is raised, but just below T_c, it exhibits a sharp peak before falling rapidly to zero at T_c. This odd behavior is not present in data taken by Kossler's group[37] in a saturated sample, and we believe that it is due to macroscopic effects in a multidomain sample.

3. Relaxation in Polycrystalline Ni

In their original letter[35], Kossler's group presented data on the temperature dependence of the muon transverse relaxation time T_2, in ferromagnetic polycrystalline Ni. The measured values of T_2 are of the order of .2 μsec. In this section I discuss the origin of this relaxation and its temperature dependence.

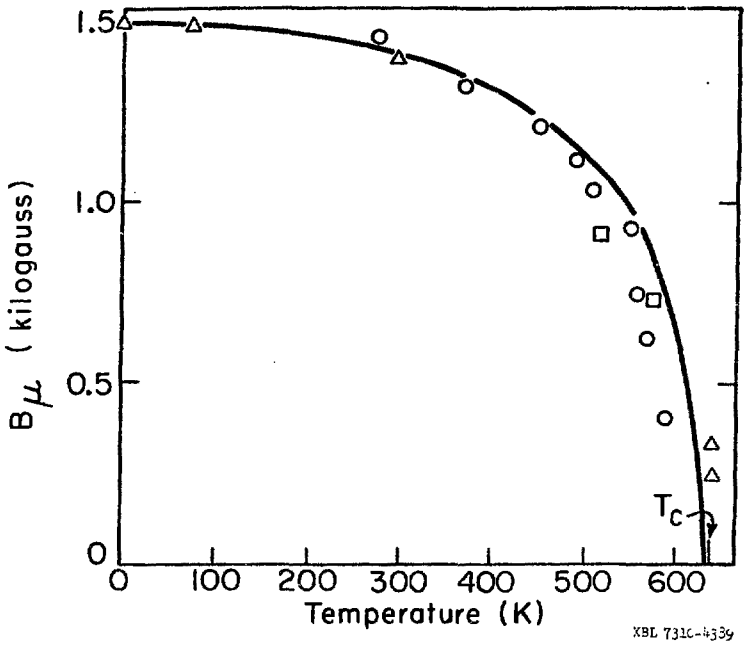

Figure 7. The local field B_μ at the muon site in nickel vs. temperature. The triangles and squares are our single crystal and polycrystal data, and the circles are Kossler's polycrystal data. The solid curve is from normalized magnetization data in Ni of reference 64.

Kossler's group reported that no precession could be observed below room temperature in their polycrystal. We managed to observe very short-lived ($T_2 \simeq 45$ nsec) precession in our polycrystal at temperatures as low as 77K, but in a single crystal, we saw long-lived ($T_2 > 1$ μsec)[65] precession even at 0.12 K. This difference between the polycrystal and single crystal strongly suggests that the existence of crystallites provides an effective relaxation mechanism.

If T_2 is expressed as an implied field inhomogeniety ΔB according to the relation $\Delta B = \frac{2}{\gamma_\mu T_2}$, Kossler's and our polycrystal data and our single crystal data may be presented as ΔB versus T as in Figure 8. Also included in the figure is data from an NMR experiment of Streever and Bennett[66] on the Ni^{61} resonance in polycrystalline Ni and data from a NMRON experiment on Co^{60} in single crystal Ni by Barclay[67]. The general agreement of the values of ΔB as measured by NMR and μ^+ in a polycrystal is significant. If ΔB were caused by strains, it would scale something like the field at the probe. The field at a Ni^{61} nucleus is 50 times the field at a μ^+. The approximate equality of ΔB as measured by these two probes implies that ΔB is the result of macroscopic field inhomogenieties and not strains.

These macroscopic field inhomogenieties are probably the result of magnetic surface charges on the interfaces of the randomly oriented crystallites. The orientation of the crystallites influences the direction of the local magnetization via the anisotropy field. From the mismatch of the crystalline axes at a crystallite interface, a similar mismatch in local

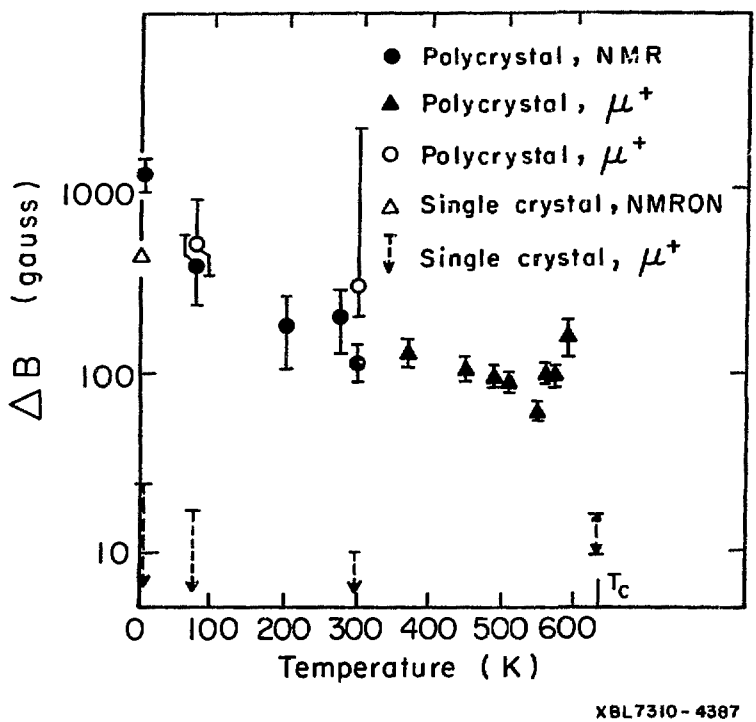

Figure 8. The linewidths ΔB observed in nickel by various techniques.

magnetizations arises. Since the magnetization is discontinuous at the boundary, magnetic charges will appear, causing the observed ΔB.

Some consequences of this model should be readily visible. As the external field is increased, the local magnetizations in the various crystallites will orient themselves parallel to the external field direction. This will have the effect of decreasing the degree of magnetization discontinuity and hence ΔB. Kossler's group noticed[35] that as the temperature was lowered to room temperature, precession could only be observed if the external field was increased.

A second consequence involves the effect of temperature. Since the magnetization and the anisotropy field decrease[64,68] as the temperature increases toward the Curie point, the local magnetizations shrink and align more easily with the external field as the temperature increases. Thus, the effect of higher temperature will be a decrease in ΔB. This is the observed dependence (see Figure 8) up to within 70 degrees of the Curie point.

Kossler's group noticed a sharp rise in ΔB as the temperature was increased above T_c - 70K. It has been suggested[69] that this is caused by critical spin fluctuations near the transition temperature. It is reasonable to assume that such fluctuations will have some effect in this temperature region (critical spin fluctuations are definitely observed just <u>above</u> T_c, as discussed in a later section), but it should be remembered that in this temperature range, the field at the muon is strongly temperature

dependent (see Figure 7). Hence, a temperature inhomogeniety or drift ΔT will produce a relaxation time $T_2(T) = \frac{2}{\gamma_\mu \Delta T \left.\frac{\delta B_\mu}{\delta T}\right|_T}$.

In Figure 9, I present a plot of ΔT, as inferred from the slope of $B_\mu(T)$ and the measured relaxation rate, versus temperature. We see that a temperature uncertainty of 12K would be sufficient to explain the observed rise in ΔB near T_c. Since the sample used by Kossler's group[35] was a large plate of Ni, a temperature uncertainty of 12K is not unreasonable. Further indication that this rise in ΔB is not due to critical spin fluctuations comes from our observation of a 2 μsec relaxation time in a small single crystal sample at 2 and 5 degrees below T_c. As shown in Figure 9, these measurements imply a temperature uncertainty of about 0.4K, which was also the experimentally measured temperature inhomogeniety across the sample. We have to conclude that to date, no evidence exists for observable critical spin fluctuations below T_c.

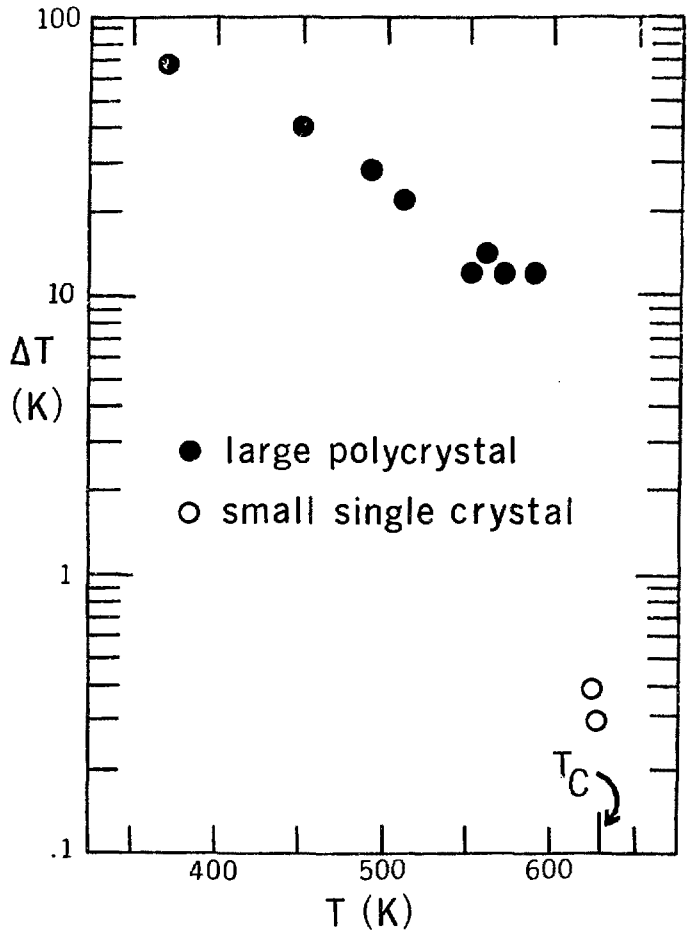

XBL 753-617

Figure 9. The temperature uncertainty ΔT required to produce the observed μ^+ relaxation times in Ni. The true temperature uncertainties appear to be 12 K for the large sample and 0.4 K for the small one.

C. Interpretation

1. 4s Screening Model for B_{hf}

We have seen that the hyperfine field predicted by a "very naive" no-screening picture agrees perfectly with experiment. But, the effect of screening on the charge density at a positive impurity in a metal was shown to be substantial. The success of the no-screening picture must be made compatible with the screening of the μ^+ by the conduction electrons of Ni.

The conduction band of Ni consists of 3d and 4s electrons[70]. The magnetic moment distribution in ferromagnetic Ni has been measured by Mook[62] and is shown in Figure 10a. Localized regions of large positive moment density are surrounded by a small negative interstitial moment density.

It should be noted that most band structure models[71-73] which consider both d- and s-electrons as itinerant cannot explain the existence of large regions in the crystal where the spin density is opposite to the majority spins. This is because the exchange splitting of <u>all</u> electrons tends to have the same sign, throughout the Brillouin zone. One notable exception is the work of Connolly[74], who through a self-consistent calculation obtains an s-electron exchange splitting opposite in sign to that of the d-states.

It is in any case probable that the negative moment density in the interstitial region of nickel (Figure 10a) is due to the 4s-electrons and that the more localized, positive moment is due to the 3d-electrons. We carry this to the extreme in a simple

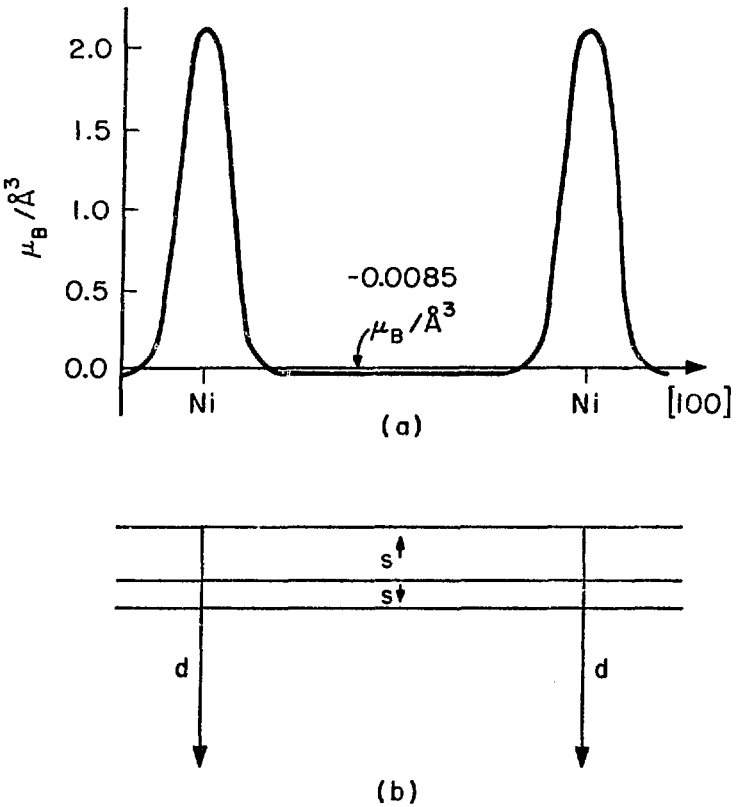

XBL 746-3442

Figure 10. a) Magnetic moment density along the [100] direction in ferromagnetic Ni as measured[62] by neutron scattering. b) Schematic diagram of spin distribution according to a simple model.

model which treats the 3d-electrons as perfectly localized on the nickel cores and the 4s-electrons as forming a free-electron gas. The density of this free-electron gas may be estimated using the atomic density of Ni and the fact[70] that each nickel core contributes 0.54 electrons to the 4s-band. This gives a uniform unperturbed 4s-electron density $n_o = 4.9 \times 10^{22}$ cm^{-3}. A schematic diagram of the unperturbed spin densities according to our model is shown in Figure 10b.

The 4s-electrons move to screen the μ^+, forming a screening cloud with a radius given roughly by the Fermi-Thomas screening length $r_s = (E_F/6\pi n_o e^2)^{1/2} = 0.6\text{Å}$, where E_F is the Fermi energy. Since the muon-nearest-neighbor nickel distance is 1.8 Å, all screening is by 4s-electrons in this model. From the earlier calculation of n(o) (Figure 5) we can find the charge density at the μ^+ in the 4s-free-electron gas. We find $n(o)/n_o \sim 5$ for the calculated 4s-density.

A simple picture predicts that the screening cloud has the same proportion of spin up and spin down electrons as the unperturbed state. Since the very naive picture of no screening gives the correct hyperfine field, this direct proportionality hypothesis will give too large a field (by a factor 5).

Consider now the form of the total energy of the free 4s-electrons. This includes: kinetic energy, s-d exchange energy, s-s exchange energy, and correlation energy. Thus, the energy density in the unperturbed case is:

$$\varepsilon_o = \frac{1}{V} \quad [E_{ke} + E_{sd} + E_{ss} + E_c],$$

where V is the volume of the sample. For the moment, we ignore

the terms E_{ss} and E_c and break E_{ke} and E_{sd} into spin up and spin down components:

$$\varepsilon_o = A\, n_o^{5/3} \left[(1+\zeta)^{5/3} + (1-\zeta)^{5/3}\right] + \mu_B H_{sd}\, n_o\, \zeta$$

Here, $A = \frac{3}{20}(3\pi^2)^{2/3} \frac{\hbar^2}{m} = 1.44 \frac{\hbar^2}{m}$, and $\zeta = \frac{n^{\uparrow} - n^{\downarrow}}{n_o}$. The first term is kinetic energy and comes from summing free electron states for the two spin orientations up to the Fermi level. In the second term, it is assumed that the effect of the s-d exchange interaction can be approximated by a Zeeman interaction with an effective, uniform, exchange field, H_{sd}.

The equilibrium value of the polarization, found by minimizing ε_o with respect to ζ, is $\zeta_o \propto -H_{sd}\, n_o^{-2/3}$. For the unperturbed case, $\zeta_o = 0.85/4.9 = 0.17$; the value of H_{sd} is fixed to give this polarization. One finds that $H_{sd} \sim -10^8$ G, a field of the order of normal Weiss fields but with the opposite sign.

The μ^+ is now introduced, and we assume that its Coulomb field does not effect the magnetic terms in the hamiltonian. We also assume a "local" approximation, i.e., ε_o goes to $\varepsilon(x)$ as n_o goes to $n(x)$ and ζ_o to $\zeta(x)$; the kinetic and magnetic energies at the point x depend only on the charge and spin densities at point x. The charge density $n(x)$ is determined by Coulomb effects, with a negligible magnetic contribution.

It is only the region near the μ^+ that is of interest, so $\varepsilon(o)$ is minimized with respect to $\zeta(o)$ to find the equilibrium polarization at the μ^+. One may then investigate how $\zeta(o)$ changes with $n(o)$ (i.e., what the relation is between the charge density and spin polarization at the μ^+. It is convenient to define two

quantities: $\rho_s = \frac{n(o)}{n_o} \frac{\zeta(o)}{\zeta_o}$ and $\rho_q = \frac{n(o)}{n_o}$, the relative spin and charge densities, which compare the perturbed and unperturbed states. The success of the very naive picture implies that the true value of ρ_s must be close to 1, and the calculation of the Lindhard screening implies that ρ_q must be ~ 5. From a plot of the calculated relationship between ρ_s and ρ_q (Figure 11), it is clear that the model is a considerable improvement over the direct proportionality hypothesis ($\rho_q = \rho_s$). When the effects of s-s exchange and correlation[59] are taken into account according to generally accepted schemes $\{E_{ss} = \frac{-3}{8} \left(\frac{3}{\pi}\right)^{1/3} e^2 n_o^{4/3} [(1+\zeta)^{4/3} + (1-\zeta)^{4/3}]$ and

$E_c = \frac{-.031}{12} \frac{e^4 m}{\hbar^2} n_o [(1+\zeta) \log (1+\zeta) + (1-\zeta)\log(1-\zeta]\}$

the agreement improves slightly (see Figure 11).

However, we have made a serious error in using the local approximation in the expression for the energy density in the perturbed state. The local approximation can only be valid when changes in charge density occur slowly over a typical electron wavelength $\lambda \sim 1/k_F \sim a$, where a is the lattice constant. But the charge density near the μ^+ changes drastically in a distance $r_s = 0.6$ Å $= a/6 < a$. Thus the local approximation is not valid, and a better (i.e.,non-local) theory is called for.

Among the advantages that a non-local extension of the model would bring is the possibility of a non-uniform s-d exchange field $H_{sd}(x)$. H_{sd} would be stronger in the vicinity of the Ni cores where the s-d overlap is greatest, and it would have a minimum at the interstitial site. The substantial exchange field near the cores could, in a non-local theory, produce the observed

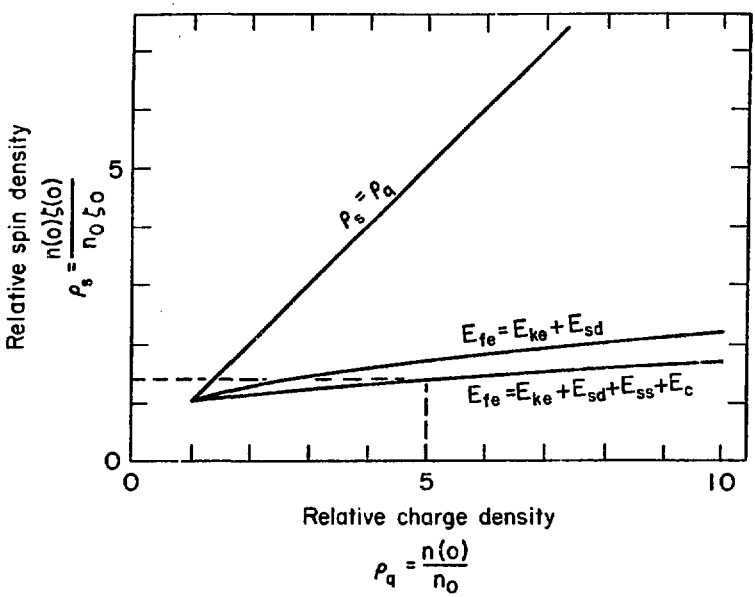

XBL 746-3443

Figure 11. Calculated relationships between the relative charge and spin densities (ρ_q and ρ_s) at the muon site. ρ_q and ρ_s are the charge and spin densities at the μ^+ normalized to the unperturbed, or μ^+-absent, situation. The straight line $\rho_s = \rho_q$ represents the "direct proportionality" hypothesis, while the remaining curves are the result of model calculations involving the designated terms in the expression for the free-electron energy E_{fe}.

interstitial spin polarization even though the exchange field here is small. Then, as the μ^+ pulls in charge, the displaced electrons would feel a weaker exchange field, and the spin density at the μ^+ would be decreased from the local approximation value. This is the desired direction of change (see Figure 11), but a quantitative discussion must await an improved calculation.

We hope, however, that the main theses of our argument will hold up to closer scrutiny. These are: 1) The neutron diffraction data correctly give the moment density, and the negative interstitial moment is from quasi-free 4s-electrons. This implies an antiferromagnetic s-d exchange interaction analagous to that found in rare earths[75]. We believe the μ^+ result and our simple theory support the neutron work. 2) The 3d-electrons participate only weakly in screening the μ^+ as if they were highly correlated on each Ni core, moving essentially as a localized unit. Such a high degree of correlation is evident[76] in NiO. 3) The kinetic energy increase accompanying a build-up of one spin orientation in the screening cloud keeps the spin density at the μ^+ low while the charge density increases.

2. Knight Shift at the μ^+ in Normal Metals

An extension of the theory just developed for the hyperfine field at the μ^+ in Ni may be made to the case of Knight shifts seen by positive muons in normal metals. This is accomplished simply by replacing the exchange field H_{sd} by the known applied external field B_o. It is now this external field which serves to polarize the screening electrons. Since ζ_o is then proportional to this external field, so is the hyperfine field at

the μ^+, which appears to shift the external field. This is the well known Knight shift ΔB. The results of a calculation of $\Delta B/B$ for various values of n(o) are presented in Figure 12a. The rise at low densities found when s-s exchange and correlation are included is known as the exchange enhancement of the spin susceptibility.

Data of Knight shifts of μ^+ precession frequencies of Hutchinson et. al. [24] (Figure 12b) follows the general shape of the exchange enhanced theoretical curve, although the quantitative agreement is poor.

3. Local Fields in Iron and Cobalt

The local field at the μ^+ in polycrystalline iron was measured by Kossler's group[36] as a function of temperature. Their results extrapolated to zero temperature give a value of B_μ of -4.1 kG. The sign has been determined by the Russian group[43].

Since the experiments were performed below saturation, the external field was compensated by the demagnetizing field. The Lorentz field at low temperature is 7.3 kG. The face-centered interstitial sites in the bcc iron lattice (the assumed μ^+ stopping sites) do not have cubic symmetry, and thus they have substantial dipolar fields. A classical calculation of these fields (ignoring possible pseudo-dipolar enchancement) gives +18 and -9 kG. Because there are twice as many of the second type of site, rapid μ^+ diffusion averages the dipolar field to zero. From the Russian data[27] cited in an earlier section, it appears that the μ^+ is indeed hopping rapidly at temperatures above 100 K

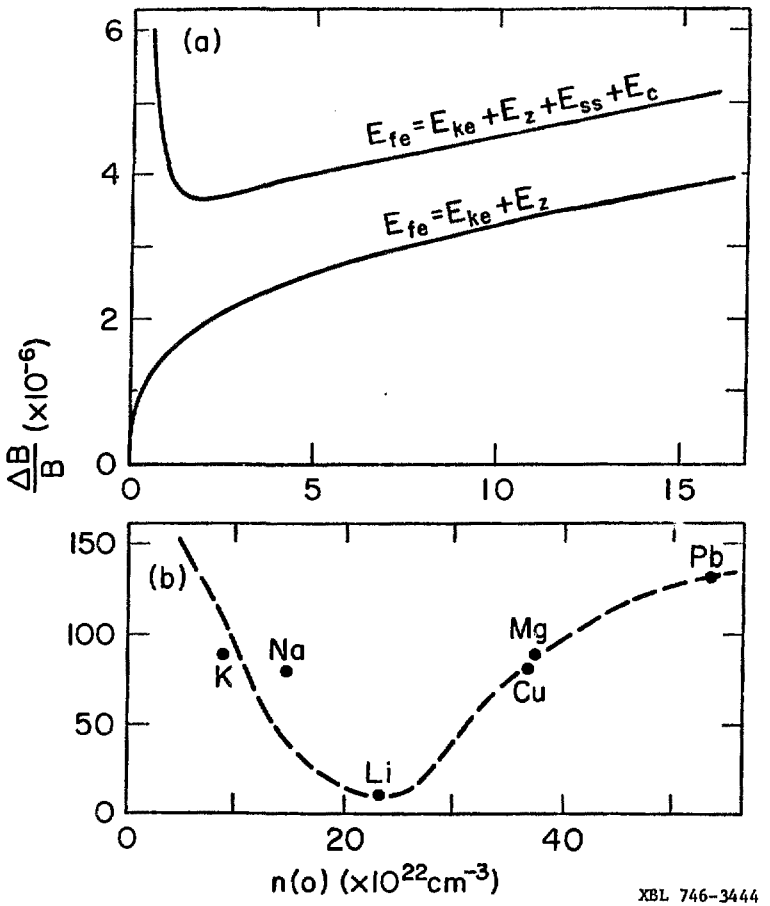

Figure 12. a) Calculated dependence of the μ^+ Knight shift ($\Delta B/B$) on the free-electron charge density at the muon n(o). The two curves represent calculations involving the designated terms in the expression for the free-electron energy E_{fe}. E_z is the Zeeman energy of the free electrons in the externally applied field. b) Knight shift data[24] of μ^+ in various metals. Here, n(o) is the free-electron density at the μ^+, calculated by the Lindhard method as described in the text.

(Kossler's data was taken above 300 K).

The only contributions to B_μ are then the Lorentz field and the hyperfine field, implying a hyperfine field of -11.4 kG. An attempt may be made to apply the "very naive" or no-screening theory to the hyperfine field in iron using neutron diffraction data of Shull and Mook[77].

The neutron diffraction data in iron shows a substantial positive local magnetization m_{loc} at the face centered site, but m_{loc} varies rapidly with position, going negative in a region around the face-centered site, then going positive again at the iron cores. A negative m_{loc} is required to explain the measured negative hyperfine field. It appears that the simple theory developed for Ni does not work for Fe; one needs to allow the μ^+ to sample the neighboring regions of negative m_{loc}.

This may be accomplished in one of two ways. A non-local theory would allow an electron drawn into the muon's screening cloud from a region of negative m_{loc} to retain its negative polarization, contributing to a negative hyperfine field. Alternatively, the muon itself could be allowed to rattle around in the interstitial site, sampling the regions of negative m_{loc} and performing some sort of volume average of the interstitial spin polarization. Such an effect has been suggested[9] to explain the temperature dependence of the Knight shift of H in Pd.

The experimental picture for μ^+ in iron is at present somewhat confused. B_μ has been measured in a polycrystalline sample at room temperature by three groups. Kossler's[36] value (-4.1 kG) disagrees with both the Russian[42] value (-3.50 kG) and our value

(-3.46 kG). It appears that there is some sample dependent effect.

We have recently observed precession in single crystal iron at room temperature. The crystal was oriented with the [111] axis parallel to the applied field, and it was just below magnetic saturation. The internal field was -3.39 kG, which again disagrees with Kossler's polycrystalline value.

We performed short runs with other orientations of the crystal ([100] and [110]), and no precession was observed. These results must be regarded as preliminary at this time because of poor statistics. It is interesting to note that only when the magnetization in single crystal iron is along the [111] axis will all interstitial dipolar fields be equivalent.

The measured local field B_μ in polycrystalline Cobalt[42] is ± 0.86 kG at room temperature (the sign is unknown at present). Since hcp cobalt has a c/a ratio which is imperfect[70] ($(c/a)_{Co}$ = 1.622, $(c/a)_{perfect}$ = 1.633), dipolar fields will exist at both the octahedral and tetrahedral interstitial sites. A classical calculation of these fields gives -0.43 and + 0.30 kG for the octahedral and tetrahedral sites respectively (the easy axis is along the c-axis). The Lorentz field at room temperature is 5.86 kG, so the extracted values of the hyperfine field range from -4.57 to -7.02 kG depending upon which sign is taken for B_μ and which type of site is assumed.

Neutron diffraction data for cobalt[78] indicates a spatially dependent local magnetization similar to that found in Ni, with a flat, negative magnetization at and near the interstitial site. The measured value of m_{loc} in this region is -0.12 $\mu_B/\text{Å}^3$ or

-1.11 kG. From m_{loc}, one can use the "very naive" picture developed for Ni to predict a hyperfine field of $8\pi m_{loc}/3 = -9.30$ kG.

The similarity of the spatial distribution of m_{loc} between Co and Ni and the success of the "very naive" picture in Ni prompts me to put some faith into this predicted hyperfine field. The discrepancy between this result and the range of values computed from experiment may lie in the fact that so far, only a classical (non-pseudo-dipolar enhanced) calculation of the dipolar fields has been performed. Pseudo-dipolar enhancement could significantly change the magnitude and even the sign of the dipolar fields.

A survey experiment searching for μ^+ precession in single crystal cobalt has been performed[37], and no signal was seen. This result is unexplained.

IV. μSR in Ni; $T \approx T_c$

A. THEORY

1. The Correlation Time Approach to μ^+ Relaxation in Ni

As the temperature of the Ni sample is increased, the saturation magnetization decreases, going to zero at the Curie temperature (T_c = 630 K). At this point, nickel becomes paramagnetic, and the average local field at the μ^+ is simply the externally applied field.

But just above T_c, remnant ferromagnetism exists in the form of clusters of ordered spins. The lifetimes and sizes of these clusters are described[79] by temperature dependent correlation times and lengths.

This fluctuation of the Ni spins causes the instantaneous value of B_μ to fluctuate. It is well known[7] that the effect of a fluctuating local field on a magnetic probe such as the μ^+ is to produce relaxation. Thus one might expect to find a temperature dependent relaxation rate for the μ^+ in Ni just above T_c. We estimate the size of this effect in the following discussion, starting from the concept of a Ni spin correlation time.

The spin correlation time τ_c is defined[80] via the spin autocorrelation function: $\tau_c \sim \int_{-\infty}^{\infty} \langle S_z(t)\, S_z(o)\rangle \,/\, \langle S_z(o)\, S_z(o)\rangle \; dt$ where S_z is the spin operator of one Ni core and the brackets imply a thermal average. In the correlation time approach, the meaning of τ_c is extended to describe correlations between different spins as well; we assume that all the Ni spins fluctuate randomly at an average frequency $1/\tau_c$.

If each of N mutually uncorrelated spins produces a magnetic field of strength ω/γ_μ at the μ^+, fluctuations of correlation time τ_c will relax the μ^+ spin at a rate given approximately by: $\frac{1}{T_2} \simeq N\omega^2\tau_c$; for $\omega\tau_c << 1$.

Concentrate for the moment on the temperature region $(T-T_C)$ greater than 70K. Microwave studies have established[81] that at these temperatures effectively all correlation between Ni spins is destroyed, and they fluctuate with a correlation time $\tau_c \sim \frac{1}{\omega_e} \sim \frac{\hbar}{J} \sim 2 \times 10^{-14}$ sec. Here ω_e is the exchange frequency, and J is the exchange energy.

Two magnetic interactions responsible for ω suggest themselves immediately: (1) the isotropic contact interaction of the μ^+ with its screening cloud of (polarized) electrons, and (2) the classical dipolar interaction with the neighboring Ni cores.

The strength of the contact interaction may be inferred from the measured[39] hyperfine field at the μ^+ in the ordered state, $B_{hf} = -0.66$kG. The octahedral site has N = 6 nearest neighbors, and we make the assumption that they share equally in the interaction, each contributing -0.11kG. Thus, $\omega_{cont} = \frac{\gamma_\mu B_{hf}}{N} \simeq 10^7$ sec^{-1}, where γ_μ is the gyromagnetic ratio of the muon. This implies a relaxation rate

$$\frac{1}{T_2}_{cont} \simeq N\omega_{cont}^2 \tau_c \simeq 10 \text{ sec}^{-1}.$$

μ^+ relaxation on this time scale would be unobservable.

Although the dipolar fields from neighboring Ni cores

vanish by symmetry at the octahedral site in the ordered state, dipolar fields from fluctuating spins can cause relaxation when the cubic symmetry is destroyed by the disappearance of spin correlation. In this case, ω is given by (for nearest neighbors):

$$\omega_{dip} \approx \frac{\gamma_\mu \mu_{Ni}}{(a/2)^3} \approx 10^8 \text{ sec}^{-1},$$

where $\mu_{Ni} = 0.6\ \mu_B$ is the magnetic moment of a Ni core and a is the lattice constant. Since ω_{dip}^2 for neighbors further removed from the μ^+ drops off rapidly with distance, we consider only the nearest neighbor contribution: $\frac{1}{T_2}_{dip} \approx N\omega_{dip}^2\ \tau_c \approx 10^3 \text{ sec}^{-1}$ which is also to small to be observable.

It is often the case that in addition to the isotropic contact interaction between the spins of a magnetic material, there exists a contact interaction with dipolar symmetry. This "pseudo-dipolar" enhancement of the classical dipolar field is known[81] to be the source of the ferromagnetic resonance linewidth and the magnetic anisotropy in Ni. It has been suggested[82] that a pseudo-dipolar enhancement of ω_{dip} by a factor 10 may not be unreasonable, in which case the relaxation would be visible.

As the temperature is lowered toward T_C, the Ni spin correlation time increases, becoming infinite at the transition. This would increase the relaxation rate expected for the μ^+.

It would be of interest to observe critical μ^+ relaxation and to compare the experimental temperature dependence of τ_c with that determined using other probes[80].

2. The Critical Exponent β

It has been shown experimentally and theoretically[83,94] that

as the temperature approaches T_C from below, the saturation magnetization obeys a simple law:

$$M_s(T) \propto \left(\frac{T_C - T}{T_C}\right)^{\beta} ; \quad T \lesssim T_C,$$

where the critical exponent β has a value close to 0.3. The theory of the μ^+ hyperfine field B_μ presented earlier[40] is compatible with the assumption that $B_{hf} \propto M_s(T)$. Making this assumption and noting that $B_\mu = \frac{4\pi M_s}{3} + B_{hf}$, we see that the local field at the μ^+ is proportional to $M_s(T)$, and we hence have an opportunity to measure the critical exponent β with a μSR experiment.

B. EXPERIMENTAL RESULTS

1. Samples and Ovens

We have performed a series of experiments observing the precession of positive muons stopped in single crystal Ni samples held at temperatures close to and above the Curie temperature T_C. It is of interest to determine the dependence of B_μ on temperature as T_C is approached from below and to study the temperature dependence of the μ^+ spin relaxation time as T_C is approached from above.

Studying the critical region around T_C requires a reliable method of temperature monitoring and control. These problems are greater for the case of μSR than for some other techniques, because, in order to stop enough muons, the samples must be fairly large. In addition, to allow the entrance of the μ^+ and to minimize stops in the oven walls, thin windows and shields must be used.

We have used three different sample-oven systems in search of a reliable design. The first oven was designed and built by the group from the University of Tokyo. It consisted of a rectangular prism of single crystal Ni 1/2 x 1 1/2 x 2 1/2" surrounded on the four thin edges by four peices of porous ceramic tile. The crystal was secured inside the square of tiles by small ceramic standoffs at four points. The tiles were held together by a non-inductive winding of non-magnetic nichrome heater wire which passed through long holes drilled lengthwise through the tiles. Molybdenum shields fit into grooves in the tiles and covered the two open faces of the sample. Then the

entire assembly was fit into a polished stainless steel box. This box, in turn, was tied to a stainless steel bar, which supported the box in a vacuum can. A mechanical pump maintained a pressure of about 40 microns, and 2 amps of dc current was passed through the nichrome heater wire. The temperature was measured at two points via Pt-Pt/Rh 13% thermocouples securely bolted to the crystal, and the heater current was controlled by an Chkuza Electric Co. model EC-7 temperature controller.

The idea of this design was to minimize the conduction of heat to the sample (via the ceramic standoffs), the convection of heat to the sample (via the vacuum), and the radiation losses from the sample to the vacuum can (via the molybdenum and stainless steel radiation shields). The heating of the sample was to occur principally via radiation from the hot ceramic tiles. With this oven, the temperature inhomogeniety near T_c was about 1.5 K across the sample. The drift with time of the temperature was less than 0.5 K during the course of a run.

It was discovered that due to conduction losses along the stainless steel bar, one of the ceramic tiles was significantly colder than the other three. This produced uneven radiation heating of the crystal. It was also decided that the vacuum should be improved.

The next model of the oven used the same crystal and heater assembly, but this time it was mounted on long thin stainless standoffs. Also, a 2" diffusion pump was added which gave a vacuum of less than 1 micron. The temperature monitoring and control was the same as for the previous model. The measured temperature inhomogeniety was about 1 K.

These two ovens were used for the relaxation rate vs. temperature studies above T_c. The fraction of muons stopping in the parts of these ovens was about 10%.

The third oven also used the 2" diffusion pump and basically the same temperature measuring and controlling system. But in this design, the Ni crystal (this time an ellipsoid of dimensions 1/2 x 1 1/2 x 2 1/2", to minimize demagnetizing field inhomogenieties) was suspended inside a copper box (whose walls were 1/16" thick) by four fine stainless steel wires and miniature egg insulators. The box was in turn suspended by stainless wires in the center of a non-inductive winding of nichrome wire. This assembly was then surrounded by four stainless radiation shields and the vacuum can.

The idea was to heat the copper box via radiation from the heater wire. The box had a fairly uniform temperature because it was made of copper. The box then heated the crystal by radiation. It was found necessary to mount a thermocouple on the copper box so the temperature of the box, not the crystal, could be controlled. This was to avoid persistent temperature oscillations between the box and the crystal. The measured temperature inhomogeniety across the sample was 0.4 K.

This oven was used at two temperatures just below T_c and for a study of the relaxation time vs. externally applied field at a fixed temperature above T_c. Roughly 40% of the muons stopped in parts of this oven.

2. Results --- $T \lesssim T_c$

Precession was observed in a single crystal sample of Ni at the temperatures $T_c - 2\ (\pm 1)$ K and $T_c - 5\ (\pm 1)$ K in an exter-

nal field of 30 gauss, and the local fields were determined to be 246 ± 10 and 340 ± 10 gauss respectively.

If one assumes $B_\mu \propto M_s(T)$, a rough estimate for the critical exponent β may be made: $\beta = 0.35 \pm 0.2$. This value, although poorly defined, is in agreement with that found[83] with other probes in Ni and that predicted theoretically[84].

The measured μ^+ relaxation times at these two temperatures are about 2 μsec. This relaxation rate can be accounted for by the 0.4 K temperature inhomogeniety in the sample (see Fig. 9). Because B_μ has such a steep temperature dependence, the true relaxation rate (due perhaps to critical spin fluctuations) is difficult to determine in this temperature region.

3. Results --- $T > T_C$

We have measured T_2 in single crystal Ni in various external fields in the temperature range $T_C + 3$ to $T_C + 300$ K, and have found the temperature and field dependence shown in Figures 13 and 14. Notice that T_2 rises rapidly with temperature just above T_C, then remains fairly constant above $T_C + 70$ K. The effect of increasing the external field is to shorten T_2.

A sophisticated fitting program was used to extract T_2 from the experimental histogram. In the analysis of the early data (Fig. 13), the fraction of muons stopping in the parts of the oven (10%) was ignored, and a straightforward 6 parameter fit (one precession component) was performed. Data taken using the third oven (Fig. 14) required a more complicated analysis procedure. Since 40% of the muons stopped in parts of the oven, the fitting program had to take account of two precession components:

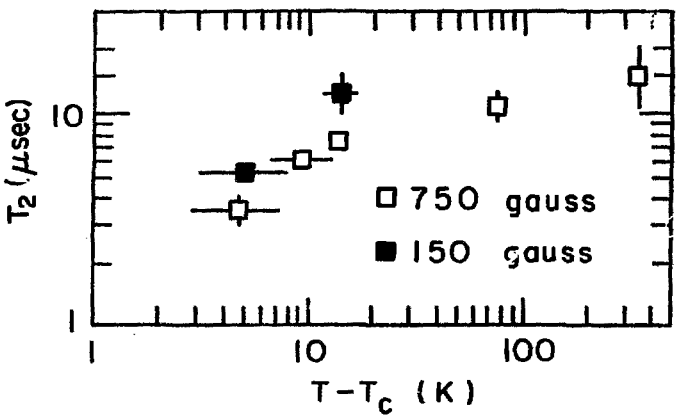

XBL7411-4586

Figure 13. The experimental dependence of T_2 on temperature and external field for muons in Ni near the Curie temperature T_c.

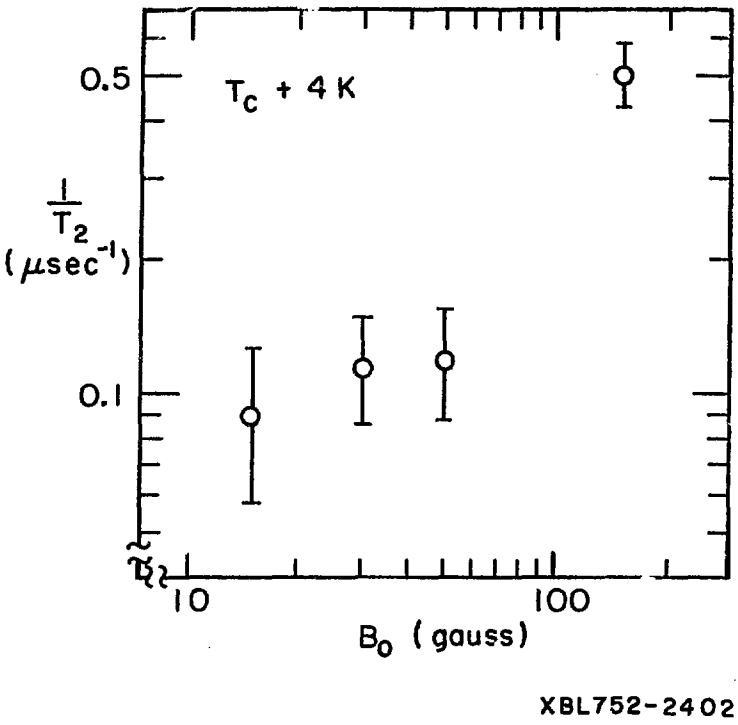

Figure 14. The experimental dependence of the μ^+ relaxation rate in Ni on external field at 4 K above the Curie temperature.

one short-lived one (in the Ni) and one long-lived one (in the oven parts). It was assumed that the precession frequencies and initial phases of these components were the same, and the computed ratio between the two asymmetries was kept fixed. At first, the relaxation time of the oven component was left as a free parameter, but it was found that fixing it at an infinite value was satisfactory.

There is a question as to the reliability of the longer T_2's measured (14 μsec). Since the μ^+ lifetime is only 2.2 usec, relaxation times this long are indeed fairly difficult to determine. The mathematical criteria involved in fixing such a long T_2 with a fitting procedure are investigated in the Appendix. More careful measurements with better statistics should undoubtedly be carried out in the high temperature region, but from the experimental evidence and from theoretical arguments, I believe the stated relaxation times are justified.

C. INTERPRETATION

1. Temperature Dependence of the Correlation Time

The strong temperature dependence found for the relaxation rate near T_c is good evidence that we are seeing the effect of critical spin fluctuations.

Figure 15 compares the μSR data with existing[80] perturbed angular correlation and neutron scattering data. From each experiment, a spin correlation time τ_c is extracted and plotted versus $(T-T_c)/T_c$. For the PAC and μSR techniques, τ_c is derived from T_2 via the relation $1/T_2 \propto \omega^2\tau_c$. The known (hyperfine) interaction strength is used for the PAC data, and for purposes of illustration, the dipolar field (without pseudo-dipolar enhancement) is used for the muon data. It should be noted that an uncertainty in ω implies an uncertainty in τ_c in only a multiplicative constant. With the pseudo-dipolar correction to ω mentioned earlier, the μSR data points join nicely onto those taken with PAC. The extraction of τ_c from the neutron data is more involved and requires fairly restrictive assumptions[80].

We see that for all three probes, as the temperature is lowered toward T_c, the correlation time increases according to the power law: $\tau_c \propto \left(\frac{T-T_c}{T_c}\right)^{-n}$ where n is 0.7 for PAC and μSR and is 1.4 for neutrons. The fact that the neutron data disagree with both the PAC and the μSR data may be due to a failure of the assumptions made in extracting τ_c from the neutron data, or it may be inherent in the manner in which the different probes sample the momentum spectrum of the critical fluctuations.

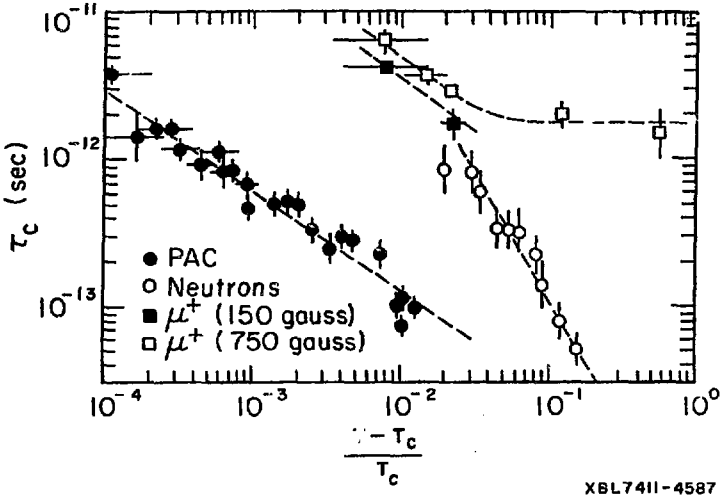

Figure 15. Extracted values of the Ni spin correlation time for different probes.

As T approaches T_c several things happen: (1) the product $\omega\tau_c$ is no longer small compared to one, and the correlation time treatment breaks down. This will only happen in a temperature region extremely close to T_c. (2) The nearest neighbors to the muon begin to correlate. When this occurs, the dipolar (and pseudo-dipolar) fields will tend to cancel by symmetry, and the contact term will gain in importance.

As seen in Figure 15, the effect of an external field is to increase the correlation time. This is the anticipated dependence since an external field is expected to stabilize the ordered state and hence to increase spin correlation. Since the PAC and neutron scattering experiments were performed in zero external field, a quantitative comparison with μSR measurements requires an extension of this work to zero field.

2. The Scattering Function Approach

The temperature dependent transition from a dipolar interaction to a contact interaction mentioned above occurs perhaps only for an interstitial probe such as the μ^+. Its existence requires (1) a weak contact interaction, (2) a strong dipolar interaction and (3) a site with cubic symmetry. It is in hopes of clarifying this effect that the scattering function approach to μ^+ critical relaxation is presented.

The scattering function approach is based on the formalism developed by Moriya[85] for NMR relaxation near T_c. According to this formalism, for a muon spin-Ni spin interaction Hamiltonian of the form: $H_{\mu j} = \vec{I}_\mu \cdot \overleftrightarrow{f}_{\mu j} \cdot \vec{S}_j$, the relaxation rate becomes:

$$\frac{1}{T_2} \propto \frac{1}{N} \sum_{\vec{k}} F(\vec{k})\, S(\vec{k},0)$$

Here, $\vec{I}_\mu$ and $\vec{S}_j$ are the muon and j^{th} Ni spins. N is the number of spins, and $S(\vec{k},0)$ is the "scattering function" for zero frequency. $F(\vec{k})$ is a form factor which contains only information about the geometry of the muon site and the strength and symmetry of the muon-Ni interaction:

$$F(\vec{k}) = \sum_{jj'} e^{-i\vec{k}\cdot(\vec{R}_j - \vec{R}_{j'})} \quad Tr[\overleftrightarrow{f}_{\mu j} \cdot \overleftrightarrow{f}_{\mu j'}]$$

Here, $\vec{R}_j$ is a vector from the μ^+ to the j^{th} Ni spin (assumed to be 1/2). Because we only consider nearest-neighbor hyperfine and dipolar interactions and because of the symmetry of the octahedral site, $\overleftrightarrow{f}_{\mu j}$ is diagonal. The sum over $\vec{k}$ is over the first Brillouin zone.

$S(\vec{k},\omega)$, the scattering function, can in principle be directly measured using neutron scattering[86]. Moriya uses an approximation[85] for $S(\vec{k},0)$, expressing it as $\chi(\vec{k})/\Gamma_{\vec{k}}$, where $\chi(\vec{k})$ is the momentum-dependent susceptability, and $\Gamma_{\vec{k}}$ is the decay rate for a fluctuation of wavevector $\vec{k}$. It should be noted that through the quantity $\Gamma_{\vec{k}}$, account is taken of the different correlation times for fluctuations with different wavelengths.

$S(\vec{k},0)$ has a maximum at $k = 0$ which grows to a singularity at $T = T_C$. This enhancement of low wavevector fluctuations is known as the diffusive mode. Moriya's approximate form for $S(\vec{k},0)$ includes only these diffusive modes.

It has recently been established[87] that propagating spin wave modes called paramagnons exist above T_C. Although these modes have maximum strength at non-zero frequencies, they probably

give a substantial contribution to $S(\vec{k},0)$ at non-zero $\vec{k}$ values. Because of the temperature dependence of the population of these modes, the spin wave contribution to $S(\vec{k},0)$ will vary with temperature. The form of the spin wave contribution to the scattering function is much more poorly understood than that of the diffusive mode.

Normalized form factors calculated for the μ^+ in the octahedral site for the case of a nearest-neighbor isotropic hyperfine interaction and for a nearest-neighbor dipolar interaction are plotted in Figure 16. The important point to note is that the dipolar form factor peaks at high $\vec{k}$, while the hyperfine form factor has a maximum at $k = 0$. This behavior may be understood as follows: since long wavelength spin fluctuations tend to maintain the correlation of the nearest neighbors of the μ^+, and because the dipolar field at the center of an octahedron of ordered spins is zero, the dipolar field from low wavevector fluctuations will be small. On the other hand, the hyperfine field is greatest when the octahedral neighbors are correlated. High wavevector fluctuations destroy this order and decrease the hyperfine field at the μ^+.

Moriya has used the calculations of Mori and Kawasaki[88] as the basis for approximate mathematical forms for $\chi(\vec{k})$ and $\Gamma_{\vec{k}}$. He then used these expressions[85] to compute the relaxation rate for the case where $F(\vec{k}) = 1$ (i.e., for the case of a nucleus interacting with a single fluctuating electron spin via an isotropic hyperfine interaction).

I have numerically performed an integration over the first Brillouin zone of the product of Moriya's scattering function for

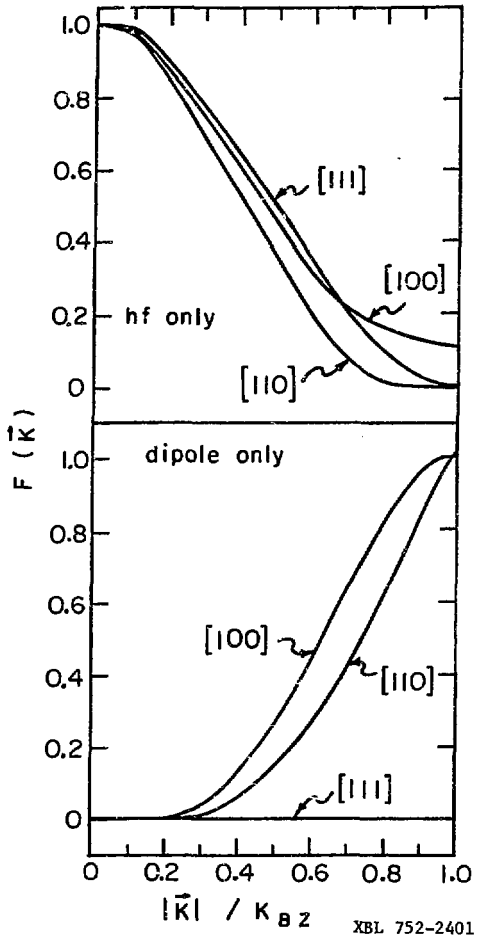

Figure 16. Normalized form factors for a μ^+ in the octahedral site of Ni. In the upper figure, only the nearest-neighbor isotropic hyperfine interaction is included, while the lower figure is for a pure nearest-neighbor dipolar interaction.

a fcc lattice and the form factor for the muon in the octahedral site. In this calculation, the hyperfine and dipolar interactions were included in the proportion suggested by the correlation time theory presented earlier. The resulting dependence of relaxation rate on temperature is shown in Figure 17. Notice that the dipolar contribution to the relaxation rate is fairly constant, decreasing by half as the Curie point is approached. The hyperfine term, on the other hand, starts small but rapidly becomes the dominant contribution. This is because the hyperfine form factor weights the low k region of $S(\vec{k},0)$ where the diffusive peak begins to diverge near T_C.

The general form of the temperature dependence agrees with the experimental data (Fig. 13). There is disagreement regarding the temperature at which the relaxation rate begins to rise and the value of the critical exponent. The data shows the rise beginning at a value of the reduced temperature $(T-T_C)/T_C \simeq 10^{-1}$, while the theory predicts 10^{-3}. The measured critical exponent is 0.7, while the theoretical value is 3/2. To some extent, these disagreements are certainly due to the approximations made within the framework of the diffusive model. Another source of disagreement may lie in the failure of the theory to account for spin waves.

It is interesting at this point to compare the μSR technique of observing critical fluctuations with those techniques which use a nuclear probe strongly coupled to a single fluctuating spin (PAC, NMR, Mossbauer effect). These probes have a $\vec{k}$-independent form factor $F(\vec{k})$, which implies that their relaxation rate will reflect some undetermined mixture of the effects of the $k \simeq 0$

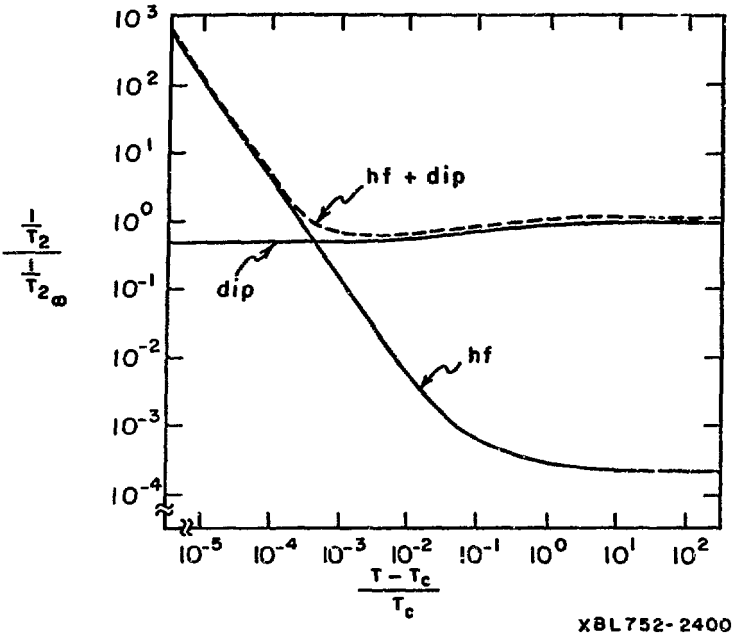

Figure 17. The normalized relaxation rate vs. reduced temperature for a μ^+ in the octahedral site in Ni according to the "scattering function approach". The relative strengths of the hyperfine and dipolar contributions were set according to arguments made in the text.

diffusive modes and the high $\vec{k}$ propagating modes. According to the theory presented for the muon, these two effects contribute to the μ^+ relaxation rate in different temperature ranges, so ideally, these two effects may be independently studied. Indeed, because the critical rise in the μ^+ relaxation rate near T_c is almost strictly due to the well understood diffusive mode, the μ^+ may prove to be the ideal probe of diffusive spin excitations near T_c.

3. Field Dependence of the Relaxation

Moriya also shows[85] how the effect of an external field on the relaxation rate may be taken into account. He finds that the principal effect of the field is to wash out the divergence in $S(\vec{k},0)$ at T_c and to decrease the diffusive peak at higher temperatures. This decrease in $S(\vec{k},0)$ causes a corresponding decrease in the relaxation rate with increasing field, which is opposite to the effect found experimentally (see Fig. 14).

However, Moriya assumes that the transition temperature remains unchanged in the presence of an external field. It has been found experimentally[89] that in a field, the transition temperature shifts upwards. This is due to the stabilization of the ordered state (i.e., enhancement of the exchange energy) by the field.

I have performed a calculation of the field effect on the μ^+ relaxation rate using Moriya's theory, taking account of the field dependent shift of the transition temperature. A linear dependence of the shift on field with a slope[89] of 10/9000 K/gauss

was assumed. The resulting curves show the correct field dependence (i.e., $1/T_2$ increases with increasing field) over a limited range of temperature and field. These results are very dependent on the exact relation between transition temperature and field.

The theory of relaxation by critical fluctuations thus becomes very complicated in the presence of an external magnetic field. This is why the other techniques which have been used in the study of critical fluctuations (neutron scattering and PAC) have concentrated on the zero field case. Our μSR experiments must be extended to zero field in order to permit a satisfactory comparison with these other techniques.

4. Effect of μ^+ Diffusion on the Relaxation Rate

A potential complication of the above picture would arise if the μ^+ were rapidly diffusing through the Ni lattice at temperatures near T_c. For sufficiently rapid diffusion, one might think that the μ^+ would "wash out" the effect of a Ni spin fluctuation. This is analagous to the case of motional narrowing of a static dipolar linewidth. But in order to wash out a fluctuation of wavevector $\vec{k}$, the μ^+ must diffuse a distance of the order of the fluctuation wavelength ($2\pi/k$) in a time short compared to the decay time of the fluctuation ($\Gamma_{\vec{k}}^{-1}$). If this criterion is not met, the μ^+ samples this fluctuation as if at rest.

It is a fortunate coincidence that those fluctuations with the shortest wavelengths also have the shortest decay times. This is stated[90] in the "slowing down hypothesis": $\Gamma_{\vec{k}}^{-1} \propto \chi(\vec{k})$. Conversely, those fluctuations which live a long time (i.e., which

remain intact during many μ^+ hops) are also those with the longest wavelengths (requiring the μ^+ to diffuse a long way to wash out the effect).

If the μ^+ were diffusing rapidly enough, it could of course wash out any fluctuation. But barring a fortuitous relation between the diffusion and fluctuation decay rates, this washing out would have to occur at all temperatures, contrary to experiment. This question should certainly be investigated more fully, but it appears that μ^+ motion may be ignored.

V. SUMMARY AND CONCLUSIONS

A. Summary

The study of ferromagnets with μSR is a rich field. In the ordered state, far below the Curie temperature, the μ^+ can be used as a microscopic magnetic probe to measure the local field due to neighboring cores and polarized screening electrons.

In ferromagnetic nickel, the dipolar fields from neighboring cores vanish because of the cubic symmetry of the μ^+ stopping site. However, the hyperfine field, from the contact interaction of the μ^+ with the polarized screening electrons, is significant. The measured value of B_{hf}, -0.66 kG, can be explained using neutron diffraction data from pure Ni and a theory which assumes that only the 4s-electrons screen the μ^+.

In the paramagnetic phase, above the Curie temperature, the local field at the μ^+ is equal to the externally applied field. But close to the transition, remnant ferromagnetism exists in the form of critical spin fluctuations.

Critical spin fluctuations in Ni near T_C rapidly relax the μ^+ spin. The relaxation rate decreases at higher temperatures. A theory based on work by Moriya[85], which clearly shows the role of the hyperfine and dipolar interactions, is in qualitative agreement with the observed temperature dependence of the μ^+ relaxation rate.

The stage is set for a new generation of careful, systematic applications of μSR to ferromagnetic materials.

B. Future Experiments

A variety of fascinating μSR experiments in magnetic materials remain to be done. It is only a matter of time until most or all of the following experiments will be performed by one of the several groups working in this field.

1) Observation of the dipolar fields in a strained Ni crystal. A direct confirmation of the μ^+ stopping site in Ni could perhaps be most easily accomplished by observing the appearence of these fields. The end of the elastic limit for stress along the [111] direction in single crystal Ni is about 200 μstrain[91]. The classical dipolar fields produced at the octahedral and tetrahedral sites for this strain are about -2 and +1 gauss respectively. Establishing the sign of the local field shift upon straining would be sufficient to determine the site. Pseudo-dipolar enhancement of the classical dipolar fields will increase the shift, and a careful measurement of the enhancement would be both useful for critical spin fluctuation studies and interesting in its own ripht.

2) Observation of two-component precession in cold single crystal iron. If the μ^+ can be frozen into two electrostatically equivalent but magnetically inequivalent face-centered sites in bcc iron, two precession components will be visible, their frequencies split by dipolar fields. This would yield information analagous to that from a strained Ni experiment.

3) Magnetic alloys in the dilute limit and near the critical concentration. The addition of a small amount of well distributed impurities to pure Ni would allow the study of μ^+

diffusion via the observation of motional narrowing of the resulting static linewidth. In addition, a study of how the muon local field in a magnetic alloy decreases as the magnetization vanishes[92] at the "critical concentration" should be undertaken.

4) A precision investigation of the temperature dependence of the μ^+ hyperfine field in a ferromagnet. One should look for deviations from perfect proportionality[93] with the magnetization.

5) A careful investigation of the temperature dependence of $B_\mu(T)$ and $T_2(T)$ near the Curie temperature. Measurements in this temperature region should be made more complete and extended to zero external field.

6) Determination of the μ^+ hyperfine field in the ordered phase of other magnetic materials including ferromagnetic alloys, antiferromagnets, and ferrimagnets.

7) μMR, or muon magnetic resonance. An experiment in which the μ^+ spin was resonantly reoriented by application of a radio-frequency magnetic field has been performed[94]. It is difficult, however, to produce a sufficiently large rf field to flip the μ^+ spin on the time scale of the μ^+ decay. The existence of the hyperfine enhancement[95] in ferromagnets could alleviate this difficulty, and one could even imagine performing a spin-echo type experiment[96] on the μ^+ in a ferromagnetic host.

C. Closing Remarks

In this dissertation I have attempted to present the

μSR technique from a solid state point of view. It is clear that μSR is a valuable solid state tool, and the advances in its application made in the future will be the result of the interest and involvement of members of the solid state community, both experimental and theoretical.

It is toward the end of fostering this interest and involvement that my colleagues and I have directed our efforts over the past few years. We have met with some depressing failures, but also with some spectacular successes. Due largely to these successes, the future existence and blossoming of this beautiful technique is guaranteed.

At the time of this writing one of the original focii of μSR physics, the 184-inch Cyclotron of the Lawrence Berkeley Laboratory, is on its financial deathbed, a victim of the mundane pressures of American economic recession. The next generation of μSR experiments will be performed at the new highly efficient "meson factories". It is the hope of the author that the lines of communication with the solid state community established through Berkeley will be maintained, strengthened and extended to the new experimental facilities.

Finally, in closing, I want to express my admiration of the human investment, both material and spiritual, in the realm of basic scientific research. In an era of human hunger, strife, and suffering, it is sometimes difficult to justify to another party, the expenditure this investment represents. But the justification to myself is obvious and immediate. The hunger, strife, and suffering on our planet are temporary. It is the curiosity of the human mind which is basic to human existence and which must be preserved.

VI. APPENDIX

In this appendix, I discuss several topics of interest regarding the two principal data reduction techniques we have used: the discrete Fourier transform and the maximum likelihood fit. Included in the discussion is a treatment of how statistical fluctuations in the experimental histogram manifest themselves in the two techniques.

A. Discrete Fourier Analysis

Fourier analysis is an elegant method of extracting the frequency spectrum from experimental data which is a function of time. In our case, the time function is the experimental histogram. Significant peaks in the frequency spectrum of this histogram represent μ^+ precession components. The moderate size of our histogram (12,000 bins), the existence of the Fast Fourier Transform algorithm[50] and the availability of a high speed digital computer make the Fourier transform technique an attractive data analysis procedure.

We start with a collection of numbers x_j, which represent successive time bins of our histogram. j is the time index. We hope to be able to express x_j as a sum of sinusoidal frequency components:

$$x_j = \sum_{k=-(N-1)}^{N} a_k \exp\frac{i\pi kj}{N} \qquad (0 \leq j \leq 2N-1)$$

where a_k is the amplitude of the component with frequency index k.

Experience with continuous Fourier transforms prompts us to guess, for a_k:

$$a_k = \frac{1}{2N} \sum_{j'=0}^{2N-1} x_{j'} \exp\frac{-i\pi kj'}{N} \qquad (-(N-1) \leq k \leq N).$$

We see that this is the correct expression by inserting it into the expression for x_j and making use of the discrete Fourier orthogonality relation:

$$\frac{1}{2N} \sum_{k=-(N-1)}^{N} \exp\frac{i\pi k(j-j')}{N} = \delta_{jj'}.$$

It is of interest to investigate the form of a_k for a simple form of x_j, namely a damped sinusoidal oscillation:

$$x(t) = Ae^{-t/T_2} \cos(\omega_o t+\phi), \quad 0 \leq t < \Delta T,$$

or, in discrete notation:

$$x_j = \frac{A}{2}\left[\exp\{i\phi + \frac{i\pi j}{N}(k_o+i\alpha)\} + \exp\{-i\phi - \frac{i\pi j}{N}(k_o-i\alpha)\}\right]$$

where

$$j = \frac{2Nt}{\Delta T}, \quad k_o = \frac{\omega_o}{2\pi}\Delta T, \quad \text{and } \alpha = \frac{\Delta T}{2\pi T_2}.$$

We adopt the notation: $k_o = n + \delta$, $(0 \leq \delta < 1)$ and $k = n + \kappa$, $(-(N-1)-n \leq \kappa < N-n)$. n gives the number of complete oscillations in the time ΔT. κ is the frequency index measured from n.

A simple calculation yields:

$$a_\kappa = \frac{A}{4N}\left[e^{i\phi}\,\frac{1-e^{2\pi i(\delta+i\alpha)}}{1-\exp\frac{-i\pi}{N}(\kappa-\delta-i\alpha)} + e^{-i\alpha}\,\frac{1-e^{-2\pi i(\delta-i\alpha)}}{1-\exp\frac{-i\pi}{N}(2n+\delta+\kappa-i\alpha)}\right].$$

The second term in this expression is a so-called "non-secular" term. It can usually be ignored for values of n not too close to 0 or 2N. If we assume $\kappa,\delta,\alpha << N$, we find:

$$a_\kappa \simeq \frac{A}{4\pi i}\, e^{i\phi}\, \frac{1-e^{2\pi i(\delta+i\alpha)}}{(\kappa-\delta-i\alpha)}, \quad (\kappa,\delta,\alpha << N)$$

$$|a_\kappa|^2 \simeq \frac{A^2}{16\pi^2}\, \frac{1-e^{-2\pi\alpha}(2\cos 2\pi\delta)+e^{-4\pi\alpha}}{(\kappa-\delta)^2+\alpha^2}.$$

The real quantity $|a_\kappa|^2$ is the Fourier power level. In the limit

of small α, this becomes:

$$|a_\kappa|^2 \simeq \frac{A^2}{4\pi^2} \frac{\sin^2\pi\delta}{(\kappa-\delta)^2+\alpha^2} \quad , \quad (\alpha \ll 1, \delta \neq 0)$$

$$\simeq \frac{A^2}{4\left[\left(\frac{\kappa}{\alpha}\right)^2+1\right]} \quad , \quad (\alpha \ll 1, \ \delta = 0) .$$

Thus, the Fourier power level has a maximum at a frequency such that $\kappa \simeq \delta$.

Although it is true that the maximum power level is a function of δ, the area under the Fourier power peak is independent of δ, as can be seen by a direct calculation (ignoring the non-secular term):

$$\sum_\kappa |a_\kappa|^2 = \frac{A^2}{8N}\left[\frac{1-e^{-4\pi\alpha}}{1-\exp\frac{-2\pi\alpha}{N}}\right] \qquad \text{(any } \alpha\text{)}$$

$$= \frac{A^2}{4} \qquad (\alpha = 0) .$$

B. Statistical Noise in a Discrete Transform

The population of each bin of the experimental histogram has a statistical uncertainty describable by a Poisson distribution. This statistical uncertainty shows itself in the discrete Fourier transform as noise peaks.

We can calculate the average noise level in a Fourier transform. Remember that the form of the noise free histogram is:

$$x_j = N_o e^{-j/j_\mu} \ [1 + y_j]$$

where $y(t) = \sum_{i=1}^{n} A_i e^{-t/T_2^i} \cos(\omega_i t+\phi_i)$. Here $t = j \times T_b$ and $j_\mu = \tau_\mu/T_b$, T_b being the time bin width and τ_μ the μ^+ lifetime (2.2 μsec). The number of bins is 2N. Any time-independent

background is assumed negligible here.

We are interested in the Fourier transform of:

$$y_j = \frac{x_j}{N_o} e^{j/j_\mu} - 1.$$

N_o may be determined via an approximate least squares fit to the histogram. The average Fourier power spectrum of y_j is:

$$\bar{P}_k \equiv \overline{|a_k|^2} = \frac{1}{(2N)^2} \sum_{j_1=0}^{2N-1} \sum_{j_2=0}^{2N-1} \overline{y_{j_1} y_{j_2}} \exp \frac{-i\pi k}{N}(j_1 - j_2) .$$

Since the histogram bins have uncorrelated populations:

$$\overline{x_{j_1} x_{j_2}} = \bar{x}_{j_1} \bar{x}_{j_2} + \delta_{j_1 j_2} (\overline{x_{j_1}^2} - \bar{x}_{j_1}^2)$$

$$= \bar{x}_{j_1} \bar{x}_{j_2} + \delta_{j_1 j_2} \bar{x}_{j_1} ,$$

because the second moment of the Poisson distribution is equal to the mean. Thus:

$$\overline{y_{j_1} y_{j_2}} = \bar{y}_{j_1} \bar{y}_{j_2} + \delta_{j_1 j_2} e^{2j_1/j_\mu} \frac{\bar{x}_{j_1}}{N_o^2}$$

and:

$$\bar{P}_k = P_k^o + \frac{1}{(2N)^2} \sum_{j=0}^{2N-1} \frac{\bar{x}_j}{N_o^2} e^{2j/j_\mu} ,$$

where P_k^o is the Fourier power in the absence of statistical noise. The second term is the average noise level.

A quantity often of interest is the signal to noise ratio P_s/P_n. The Fourier power of a signal with asymmetry A was shown to be $P_s = A^2/4$. The average Fourier power level of pure noise is:

$$P_n = \frac{1}{(2N)^2} \sum_{j=0}^{2N-1} \frac{\bar{x}_j}{N_o^2} e^{2j/j_\mu} \simeq \frac{1}{(2N)^2 N_o} \sum_{j=0}^{2N-1} e^{j/j_\mu}$$

for small A. The signal to noise ratio thus has the form:

$p_s/p_n \propto A^2 N_o$. An experiment should be designed to maximize the product $A^2 N_o$.

The probability distribution of the transform noise peaks can also be determined[97]. The effect of random fluctuations in the bin populations x_j will be an uncertainty in a_k which resembles a random walk in the complex plane of a_k. This will be rigorous as 2N approaches infinity. The distribution of a_k for pure noise is then a two-dimensional gaussian in the complex plane centered on the origin:

$$P(r) \propto e^{-r^2/2\sigma^2} \quad ; \quad r \equiv |a_k| .$$

We can now calculate the probability distribution of Fourier power peak heights:

$$P(r^2)dr^2 = P(r)dr$$

$$P(r^2) = \frac{1}{2r} P(r)$$

$$P(p_k) = 2\pi r P(r^2) = \pi P(r) .$$

Thus: $$P(p_k) = C\, e^{-p_k/c} .$$

The constants C and c are determined by normalizing the distribution and computing its mean value:

$$1 = \int_0^\infty P(p_k)dp_k = Cc$$

$$\bar{p}_k = \int_0^\infty p_k P(p_k)dp_k = Cc^2 = c .$$

For pure noise, $\bar{p}_k = \bar{p}$ is independent of k. We thus find:

$$P(p_k) = \frac{e^{-p_k/\bar{p}}}{\bar{p}} \quad ; \quad \bar{p} = \frac{1}{(2N)^2} \sum_{j=0}^{2N-1} \frac{\bar{x}_j}{N_o^2} e^{2j/j_\mu} .$$

When calculating $\bar{p}$, it is a good approximation to use x_j instead of $\bar{x}_j$. Then, with the value of N_o determined previously (e.g., by an approximate least squares fit), the expected noise

peak distribution may be determined. A coherent signal appears in the distribution of Fourier power peaks as a significant deviation from the expected noise peak distribution. In Figure 18, I plot the experimental distribution of Fourier power peaks of two actual spectra along with the distribution expected for pure noise. The isolated point in the right-hand figure indicates the presence of a significant signal.

C. A Theory of Noise in the Maximum Likelihood Fitting Procedure

Consider the negative log maximum likelihood function[51] for a histogram x_i and a theoretical average form $\bar{x}_i$:

$$F = -\sum_i \ln w(x_i, \bar{x}_i).$$

$w(x_i, \bar{x}_i)$ describes the probability distribution of the population in the i^{th} bin (assumed here, for ease of calculation to be gaussian, as would be the case for a "compressed" histogram, ie, many neighboring bins summed into a single new bin):

$$w(x_i, \bar{x}_i) = \frac{1}{(2\pi \bar{x}_i)^{1/2}} \exp \frac{-(x_i - \bar{x}_i)^2}{2\bar{x}_i}$$

Note that the width of the distribution is taken to be $(\bar{x}_i)^{1/2}$ as is the case for a compressed histogram with initially Poisson statistics.

We find that F is minimized if $\bar{x}_i = \bar{x}_i^o$ is chosen such that it most closely approximates x_i:

$$F \text{ (minimum)} = F_o = -\sum_i \ln w(x_i, \bar{x}_i^o)$$

$$F_o = \sum_i \left[\frac{1}{2} \ln(2\pi \bar{x}_i^o) + \frac{(x_i - \bar{x}_i^o)^2}{2\bar{x}_i^o} \right].$$

Consider now a second theoretical average form $\bar{x}_i'$ corres-

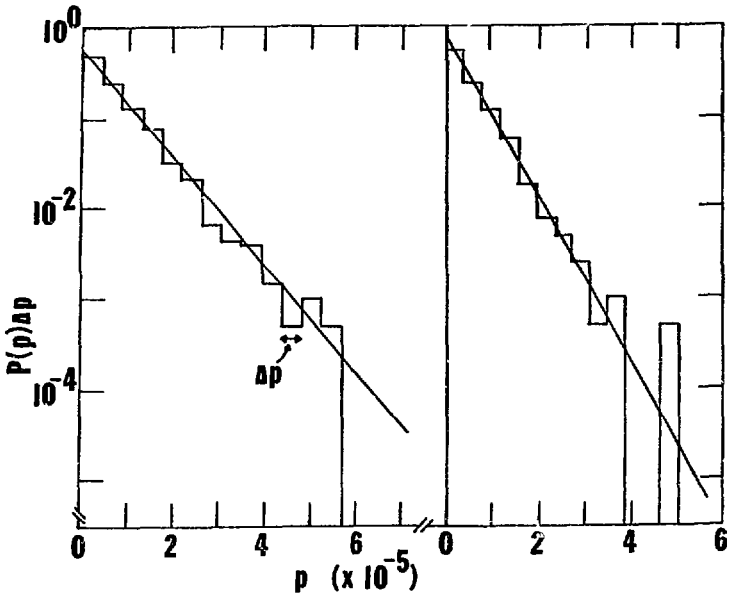

Figure 18. The experimental Fourier power peak distribution (bar graphs) and the expected distribution for pure noise (straight lines) for two actual 2048-point transforms. The isolated bar in the right-hand figure demonstrates the existence of a statistically significant signal.

ponding to values of the fitting parameters different from the optimal case $\bar{x}_i^o$. We wish to determine under what conditions we can discriminate the form $\bar{x}_i'$ from the form $\bar{x}_i^o$.

We first calculate the expectation value of the difference $f = F' - F_o$, finding easily:

$$\bar{f} = \frac{1}{2} \sum_i \left(\frac{(\bar{x}_i^o - \bar{x}_i')^2}{\bar{x}_i'} + \frac{(\bar{x}_i^o - \bar{x}_i')}{\bar{x}_i'} + \ln \frac{\bar{x}_i'}{\bar{x}_i^o} \right)$$

$$\bar{f} \simeq \frac{1}{2} \sum_i \frac{(\bar{x}_i^o - \bar{x}_i')^2}{\bar{x}_i'} \quad ; \quad \bar{x}_i \gg 1 .$$

The condition that $\bar{x}_i'$ can be distinguished from $\bar{x}_i^o$ is that $\bar{f} > \Delta f \equiv \overline{\{(f - \bar{f})^2\}}^{1/2}$. We calculate $(\Delta f)^2$ assuming the statistical independence of neighboring bins:

$$\overline{x_i x_j} = \bar{x}_i \bar{x}_j \quad ; \quad (i \neq j)$$

$$(\Delta f)^2 = \frac{1}{4} \sum_{ij} [\overline{C_i C_j} - \bar{C}_i \bar{C}_j] = \frac{1}{4} \sum_i [\overline{C_i^2} - \bar{C}_i^2] ;$$

$$C_i \equiv \frac{(x_i - \bar{x}_i')^2}{\bar{x}_i'} - \frac{(x_i - \bar{x}_i^o)^2}{\bar{x}_i^o} .$$

After a fairly tedious calculation, we find:

$$(\Delta f)^2 = \sum_i (2\bar{x}_i^o + 1) \frac{(\bar{x}_i^o - \bar{x}_i')^2}{2\bar{x}_i'^2}$$

$$(\Delta f)^2 \simeq \sum_i \frac{\bar{x}_i^o}{\bar{x}_i'^2} (\bar{x}_i^o - \bar{x}_i')^2 \quad ; \quad \bar{x}_i \gg 1 ,$$

If we let: $\bar{x}_i' = \bar{x}_i^o (1 + \delta_i)$; $\bar{x}_i^o \gg 1$, $\delta_i \ll 1$,

we find: $\bar{f} \simeq \frac{1}{2} \sum_i \bar{x}_i^o \delta_i^2$

$$(\Delta f)^2 \simeq 2 \bar{f} .$$

The condition required to be able to statistically discriminate between the two forms is: $\bar{f} > \Delta f$, or $\bar{f} > 2$.

For the case of our histogram, if $\bar{x}_i'$ differs from $\bar{x}_i^o$ in any interesting parameter (i.e., any but the normalization N_o or the background B), $\bar{f}$ will, in the limit of small asymmetry A, be proportional to the product $N_o A^2$. Thus, we again see the importance of maximizing this product. In Figures 19 and 20 I present the results of calculations of the minimum number of events required to 1) measure the precession frequency to a specified precision and to 2) differentiate between a finite relaxation time and an infinite relaxation time.

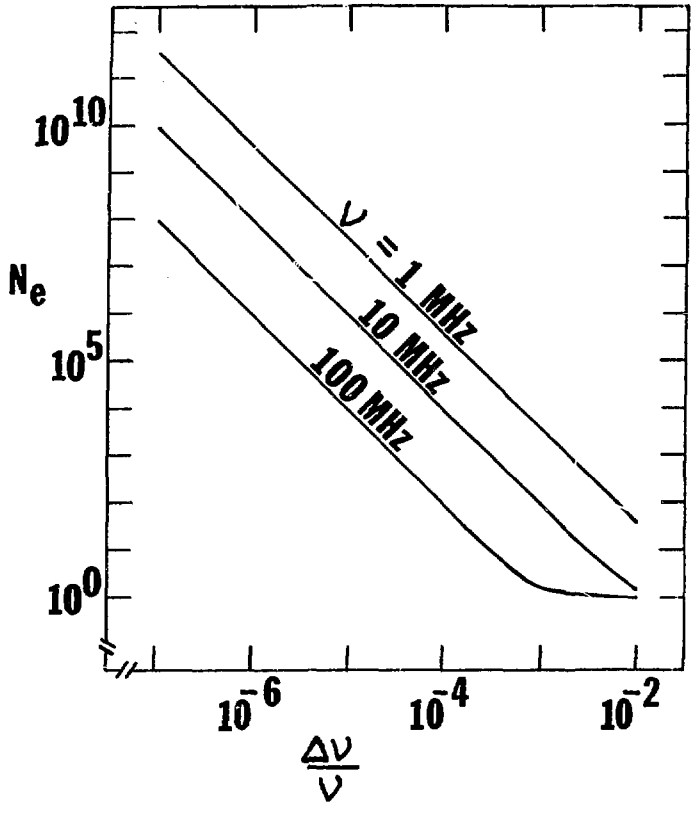

XBL 753-706

Figure 19. The number of events required to statistically discriminate a precession frequency ν from a frequency $\nu + \Delta\nu$. An infinite relaxation time and an asymmetry of 0.2 are assumed. It is also assumed that the histogram covers three μ^+ lifetimes.

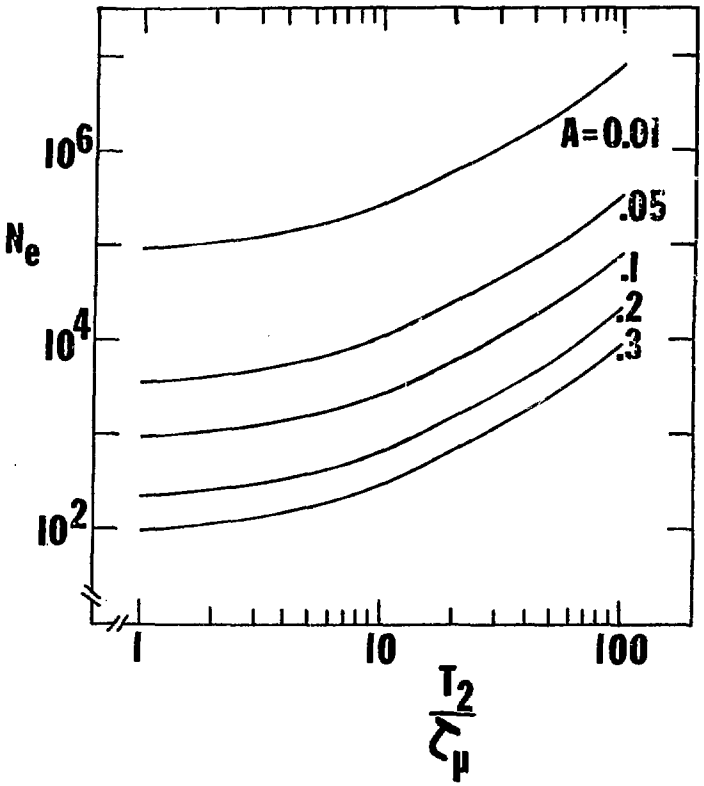

XBL 753-701

Figure 20. The number of events required in order to statistically discriminate between a finite value of T_2 and an infinite value. A is the asymmetry, and τ_μ is the lifetime of the μ^+ (2.2 μsec). This plot assumes a histogram which covers three μ^+ lifetimes.

ACKNOWLEDGEMENTS

First thanks go to Ken Crowe, my thesis adviser, who was quick with criticism and praise both in the lab and on his sailboat. It was a pleasure to be associated with him and the other members of the group. These include Jesse Brewer (the master steelheader), Richard Johnson (may all his integrals converge), Fred Gygax (connoisseur and bon vivant), and Corrine Sergent (a free spirit chained to an IBM Selectric).

Our collaboration with a group from the University of Tokyo was profitable and enjoyable. With apologies for the weekly scheduling fights, I want to thank Ken Nagamine, Toshi Yamazaki, Shoji Nagamiya, Osamu Hashimoto, and Nobu Nishida.

The experimentalist is lost without capable technical support. I wish to acknowledge the kind help of Leal Kanstein and the 184" Cyclotron crew, our computer specialists Vic Elischer and Oliver Jones, and three excellent machinists, Lou Sylvia, Carson Haines, and "Hap" Hagopian.

I can't overestimate the contributions three solid state physicists have made to this thesis, my education, and the μSR technique. Prof. Leo Falicov was a strong positive influence during the formulation of the theory for the hyperfine field in nickel. Prof. Cesare Bucci brought his deep insights to bear on the problems surrounding critical fluctuations in nickel. And, a special note of thanks goes to Prof. Alan Portis who has shown an avid interest in this work from its inception, and who has been the source of a multitude of major contributions in spite of the barrages of silly questions we always threw at him.

A note of thanks is also due my good friend and fellow graduate student Don Bethune, for helpful discussions and good times.

The patience and co operation of my thesis committee is gratefully acknowledged.

My parents bear much more of the responsibility for this thesis than that they fulfilled on my birthday. They have shown a very involved and active interest in my entire education, even past the point where the language became new to them.

Finally, I wish to thank my wife, Anne-Britt, for her patient acceptance of the realities of being married to a physics graduate student and for her constant love.

REFERENCES

1. K. M. Crowe, J. F. Hague, J. E. Rothberg, A. Schenck, D. L. Williams, R. W. Williams, and K. K. Young, Phys. Rev. D, 5, 2145 (1972).
2. J. H. Brewer, K. M. Crowe, F. N. Gygax, and A. Schenck, in "Muon Physics", edited by V. W. Hughes and C. S. Wu (Academic, New York, to be published).
3. A. Schenck and K. M. Crowe, Phys. Rev. Lett. 26, 57 (1971).
4. J. H. Brewer, K. M. Crowe, F. N. Gygax, R. F. Johnson, B. D. Patterson, D. G. Fleming, and A. Schenck, Phys. Rev. Lett 31, 143 (1973).
5. I. Isenberg, Phys. Rev. 79, 736 (1950).
6. W. D. Knight, Phys. Rev. 76, 1259 (1949).
7. A. Abragam, "The Principles of Nuclear Magnetism" (Clarendon, Oxford, 1961).
8. R. E. Norberg, Phys. Rev. 86, 745 (1952).
9. A. Fert and P. Averbuch, J. de Physique 25, 297 (1964)
10. B. Stalinski, C. K. Coogan, and H. S. Gutowsky, J. Chem. Phys. 34, 1191 (1961).
11. J. P. Kopp and D. S. Schreiber, Phys. Lett. 24A, 323 (1967).
12. H. T. Weaver, Phys. Rev. B, 6, 2544 (1972).
13. R. A. Oriani, E. McCliment, and J. F. Younghlood, J. Chem. Phys. 27, 330 (1957).
14. D. S. Schreiber and L. D. Graham, J. Chem. Phys. 43, 2573 (1965).
15. K. Tanaka and T. Hashimoto, J. Phys. Soc. Japan 34, 379 (1973).

16. A. N. Gil'manov and V. .. Fedotov, Fiz. Metal. Metalloved. 29, 1288 (1970).

17. H. Barrere and K. M. Tran, C. R. Acad. Sc. Paris 273, 823 (1971).

18. J. Bergsma and J. A. Goedkoop, Physica 26, 744 (1960).

19. E. O. Wollan, J. W. Cable, and W. C. Koehler, J. Phys. Chem. Solids 24, 1141 (1963).

20. M. A. Garstens, Phys. Rev. 81, 288 (1951).

21. D. S. Schreiber and R. M. Cotts, Phys. Rev. 131, 1118 (1963).

22. Ye. F. Khodosov, Fiz. Metal. Metalloved. 29, 415 (1970).

23. E. F. Khodosov and I. I. Khodos, Sov. Phys. Solid State 12, 2213 (1971).

24. D. P. Hutchinson, J. Menes, G. Shapiro, and A. M. Parlach, Phys. Rev. 131, 1351 (1963).

25. I. I. Gurevich, E. A. Mel'eshko, I. A. Muratova, B. A. Nikol'sky, V. S. Roganov, V. I. Selivanov, and B. V. Sokolov, Phys. Lett. 40A, 143 (1972).

26. A. T. Fiory, D. E. Murnick, M. Leventhal, and W. J. Kossler, Phys. Rev. Lett. 33, 969 (1974).

27. I. I. Gurevich, A. N. Klimov, V. N. Maiorov, E. A. Meleshko, B. A. Nikol'skii, V. S. Roganov, V. I. Selivanov, and V. A. Suetin, JETP Lett. 18, 332 (1973).

28. J. Friedel, Ber. Buns. Gesellschaft 76, 828 (1972).

29. E. Hayashi and M. Shimizu, J. Phys. Soc. Japan 26, 1396 (1969).

30. D. J. Kim and B. B. Schwartz, Phys. Rev. Lett. 28, 310 (1972).

31. D. J. Kim, Phys. Lett. 46A, 177 (1973).

32. F. Rasetti, Phys. Rev. 66, 1 (1944).

33. G. H. Wannier, Phys. Rev. 72, 304 (1947).

34. J. H. Brewer (private communication).

35. M. L. G. Foy, N. Heiman, W. J. Kossler, and C. E. Stronach, Phys. Rev. Lett. 30, 1064 (1973).

36. N. Heiman, M. L. G. Foy, W. J. Kossler, and C. E. Stronach, 19th Conf. Mag. Magnetic Materials, Boston (1973).

37. M. L. G. Foy, Ph.D. thesis, The College of William and Mary (unpublished)

38. D. E. Murnick, M. Leventhal, and W. J. Kossler, Conf. on Hyperfine Int. Det. Nuc. Rad., Uppsala, Sweden (1974).

39. B. D. Patterson, K. M. Crowe, F. N. Gygax, R. F. Johnson, A. M. Portis, and J. H. Brewer, Phys. Lett. 46A, 453 (1974).

40. B. D. Patterson and L. M. Falicov, Solid St. Comm. 15, 1509 (1974).

41. B. D. Patterson, K. Nagamine, C. A. Bucci, and A. M. Portis, 20th Conf. Mag. Magnetic Materials, San Francisco (1974).

42. I. I. Gurevich, A. I. Klimov, V. N. Maiorov, E. A. Meleshko, I. A. Muratova, B. A. Nikolsky, V. S. Roganov, V. I. Selivanov, and V. A. Suyetin, ZhETP 66, 374 (1974).

43. I. I. Gurevich, A. I. Klimov, V. N. Maiorov, E. A. Meleshko, B. A. Nikolsky, A. V. Pirogov, V. I. Selivanov, and V. A. Suyetin, ZhETF Pis. Red. 20, 558 (1974).

44. I. G. Ivanter, Sov. Phys. JETP 36, 990 (1973).

45. E. Daniel and J. Friedel, J. Phys. Chem. Solids 24, 1601 (1963).

46. C. P. Slichter, "Principles of Magnetic Resonance" (Harper & Row, New York, 1963).

47. Y. Ebisuzaki, W. J. Kass, and M. O'Keefe, J. Chem. Phys. 46, 1373 (1967).

48. B. Bergersen, E. Pajanne, P. Kubica, M. J. Stott, and C. H. Hodges, Solid St. Comm. 15, 1377 (1974).

49. B. M. Smirnov, Sov. Phys. JETP 17, 133 (1963).

50. J. W. Cooley and J. W. Tukey, Math. of Comput. 19, 297 (1965).

51. J. Orear, Lawrence Rad. Lab. report # UCRL-8417.

52. R. H. Fowler and C. J. Smithels, Proc. Roy. Soc. A160, 37 (1937).

53. A. P. Pathak, Phys. Rev. B, 2, 3021 (1970).

54. Z. D. Popovic and M. J. Stott, Phys. Rev. Lett. 33. 1164 (1974).

55. G. F. Koster and J. C. Slater, Phys. Rev. 96, 1208 (1954).

56. J. Friedel, Nuovo Cim. Suppl. 7, 287 (1958).

57. H. J. Bauer and E. Schmidbauer, Z. Phys. 164, 367 (1961).

58. F. Seitz, "The Modern Theory of Solids" (McGraw-Hill, New York, 1940).

59. C. Kittel, "Quantum Theory of Solids" (Wiley, New York, 1967).

60. J. Lindhard, Kgl. Danske Videnskab. Selskab, Mat-fys. Medd. 28, No. 8 (1954).

61. M. B. Stearns (unpublished)

62. H. A. Mook, Phys. Rev. 148, 495 (1966).

63. J. A. Osborn, Phys. Rev. 67, 351 (1945).

64. P. Weiss and R. Forrer, Ann. de Physique, Ser. 10, 5, 153 (1926).

65. Only an upper limit for T_2 can be given due to the short μ^+ lifetime and the interference of the precession signal

with a 19 MHz background signal arising from the time structure of the cyclotron beam.

66. R. L. Streever and L. H. Bennett, Phys. Rev. 131, 2000 (1963).

67. J. A. Barclay, Ph.D. thesis, Lawrence Rad. Lab. report # UCRL-18986.

68. G. Aubert, J. Appl. Phys. 39, 504 (1968).

69. W. J. Kossler (private communication).

70. C. Kittel, "Introduction to Solid State Physics" (Wiley, New York, 1971).

71. E. Zornberg, Phys. Rev. B, 1, 244 (1970).

72. L. Hodges, H. Ehrenreich, and N. D. Lang, Phys. Rev. 152, 505 (1966).

73. J. Langlinais and J. Callaway, Phys. Rev. B, 5, 124 (1972).

74. J. W. D. Connolly, Phys. Rev. 159, 415 (1967).

75. V. Jaccarino, B. T. Matthias, M. Peter, H. Suhl, and J. H. Wernick, Phys. Rev. Lett. 5, 251 (1960).

76. B. Koiller and L. M. Falicov, J. Phys. C: Solid St. Phys. 7, 299 (1974).

77. C. G. Shull and H. A. Mook, Phys. Rev. Lett. 16, 184 (1966).

78. R. M. Moon, Phys. Rev. 136, A195 (1964).

79. M. E. Fisher, Reports Prog. Phys. 30, 615 (1967).

80. A. M. Gottlieb and C. Hohenemser, Phys. Rev. Lett. 31, 1222 (1973).

81. M. B. Salamon, Phys. Rev. 155, 224 (1967).

82. A. M. Portis (private communication).

83. J. Bleck, R. Butt, R. Michaelsen, S. S. Rosenblum, and W. D. Zeitz, Conf. on Hyperfine Int. Det. Nuc. Rad., Uppsala, Sweden (1974).

84. G. W. Essam and M. E. Fisher, J. Chem. Phys. 38, 802 (1963).

85. T. Moriya, Prog. Theor. Phys. 28, 371 (1962).

86. R. D. Lowde and C. G. Windsor, Adv. Phys. 19, 813 (1970).

87. H. A. Mook, J. W. Lynn, and R. M. Nicklow, Phys. Rev. Lett. 30, 556 (1973).

88. H. Mori and K. Kawasaki, Prog. Theor. Phys. 27, 529 (1962).

89. K. M. Koch, Oest. Ingen.-Arch. 5, 278 (1951).

90. P. Heller, Reports Prog. Phys. 30, 731 (1967).

91. C. Mercer (private communication).

92. T. J. Hicks, B. Rainford, J. S. Kouvel, and G. G. Low, Phys. Rev. Lett. 22, 531 (1969).

93. K. Johansson, E. Karlsson, and L. O. Norlin, Conf. on Hyperfine Int. Det. Nuc. Rad., Uppsala, Sweden (1974).

94. T. Coffin, R. L. Garwin, S. Penman, L. M. Lederman, and A. M. Sachs, Phys. Rev. 109, 973 (1958).

95. A. M. Portis and R. H. Lindquist, in "Magnetism", vol. IIA, p. 357, edited by G. T. Rado and H. Suhl (Academic, New York, 1965).

96. E. L. Hahn, Phys. Rev. 80, 580 (1950).

97. I am indebted to J. Middleditch for this derivation.